Redox Biology 37 (2020) 101695

Contents lists available at ScienceDirect

Redox Biology

journal homepage: www.elsevier.com/locate/redox

Research Paper

α-Synuclein amplifies cytoplasmic peroxide flux and oxidative stress provoked by mitochondrial inhibitors in CNS dopaminergic neurons *in vivo*

Victor S. Van Laar [a,b,1], Jianming Chen [a,b,1], Alevtina D. Zharikov [a,b,1], Qing Bai [a,b], Roberto Di Maio [a,b], April A. Dukes [a,b], Teresa G. Hastings [a,b], Simon C. Watkins [c,d], J. Timothy Greenamyre [a,b], Claudette M. St Croix [c,d], Edward A. Burton [a,b,e,f,*]

[a] Pittsburgh Institute for Neurodegenerative Diseases, University of Pittsburgh, Pittsburgh, PA, USA
[b] Department of Neurology, University of Pittsburgh, Pittsburgh, PA, USA
[c] Center for Biologic Imaging, University of Pittsburgh, Pittsburgh, PA, USA
[d] Department of Cell Biology, University of Pittsburgh, Pittsburgh, PA, USA
[e] Department of Microbiology and Molecular Genetics, University of Pittsburgh, Pittsburgh, PA, USA
[f] Geriatric Research, Education and Clinical Center, VA Pittsburgh Healthcare System, Pittsburgh, PA, USA

ARTICLE INFO

Keywords:
Parkinson's disease
α-Synuclein
Peroxide
Glutathione
Zebrafish
Dopaminergic neuron

ABSTRACT

Convergent evidence implicates impaired mitochondrial function and α-Synuclein accumulation as critical upstream events in the pathogenesis of Parkinson's disease, but comparatively little is known about how these factors interact to provoke neurodegeneration. We previously showed that α-Synuclein knockdown protected rat substantia nigra dopaminergic neurons from systemic exposure to the mitochondrial complex I inhibitor rotenone. Here we show that motor abnormalities prior to neuronal loss in this model are associated with extensive α-Synuclein-dependent cellular thiol oxidation. In order to elucidate the underlying events *in vivo* we constructed novel transgenic zebrafish that co-express, in dopaminergic neurons: (i) human α-Synuclein at levels insufficient to provoke neurodegeneration or neurobehavioral abnormalities; and (ii) genetically-encoded ratiometric fluorescent biosensors to detect cytoplasmic peroxide flux and glutathione oxidation. Live intravital imaging of the intact zebrafish CNS at cellular resolution showed unequivocally that α-Synuclein amplified dynamic cytoplasmic peroxide flux in dopaminergic neurons following exposure to the mitochondrial complex I inhibitors MPP^+ or rotenone. This effect was robust and clearly evident following either acute or prolonged exposure to each inhibitor. In addition, disturbance of the resting glutathione redox potential following exogenous hydrogen peroxide challenge was augmented by α-Synuclein. Together these data show that α-Synuclein is a critical determinant of the redox consequences of mitochondrial dysfunction in dopaminergic neurons. The findings are important because the mechanisms underlying α-Synuclein-dependent reactive oxygen species fluxes and antioxidant suppression might provide a pharmacological target in Parkinson's disease to prevent progression from mitochondrial dysfunction and oxidative stress to cell death.

1. Introduction

Sporadic Parkinson's disease (PD) is a common and progressive neurodegenerative disease, resulting clinically in a hypokinetic movement disorder and additional non-motor manifestations. Pathologically, PD is characterized by neuronal loss and formation of Lewy bodies and Lewy neurites, α-Synuclein-immunoreactive proteinaceous inclusions found in neuronal cell bodies, axons, and dendrites in affected brain regions. The characteristic motor deficits of PD – tremor, rigidity, and bradykinesia – result from degeneration of the dopaminergic nigrostriatal projection, which seems particularly vulnerable to pathogenesis. The mechanisms underlying degeneration of susceptible neuronal groups in PD are incompletely understood; convergent evidence links abnormalities of both mitochondrial function and α-Synuclein proteostasis to downstream cell death.

Patients with PD show systemic deficits in mitochondrial respiratory

* Corresponding author. 7015 Biomedical Science Tower 3, 3501 Fifth Avenue, Pittsburgh, PA, 15213, USA.
E-mail address: eab25@pitt.edu (E.A. Burton).
[1] Contributed equally and should be considered joint first authors.

https://doi.org/10.1016/j.redox.2020.101695
Received 18 June 2020; Received in revised form 17 July 2020; Accepted 17 August 2020
Available online 22 August 2020

function, particularly complex I of the electron transport chain (ETC) [24,56]. PD brain tissue also shows decreased mitochondrial function and evidence of excessive reactive oxygen species (ROS) generation, including consumption of endogenous antioxidants [49,60], and oxidative damage to cellular macromolecules such as proteins, lipids and nucleic acids. A causative or mechanistic role for mitochondrial dysfunction in PD is supported by epidemiological links between exposure to environmental toxicants that inhibit the respiratory chain and risk of PD [65], and by cases of acute clinical parkinsonism caused by MPTP (which is metabolized in the CNS to yield MPP^+, a complex I inhibitor) [36]. Further evidence is provided by Mendelian parkinsonism phenocopies caused by loss of proteins with critical mitochondrial functions, such as Parkin and Pink1 which are centrally involved in mitochondrial quality control [46,47].

α-Synuclein is an abundant neuronal protein involved in synaptic vesicle trafficking and recycling. Mutations in the SNCA gene encoding α-Synuclein cause an autosomal dominant form of parkinsonism with prominent Lewy body pathology. In addition to missense mutations that change the biophysical properties of the protein [34,50], gene duplication [11] and triplication [62] events that result in over-expression of wild-type α-Synuclein also cause progressive parkinsonism, with a correlation between gene dose and phenotypic severity. Together with its presence in the hallmark pathological inclusions of sporadic PD [1,63], these observations support a proximate causative role for α-Synuclein in neurodegeneration. This idea is further supported by an association between sporadic PD and non-coding single nucleotide polymorphisms near to the SNCA gene that may modulate α-Synuclein expression levels [55,61], and by evidence suggesting that pharmaceutical exposures that alter α-Synuclein expression may also modulate PD risk [45]. α-Synuclein aggregates readily; evidence of stereotyped and possibly sequential patterns of aggregate deposition in the CNS [6], in addition to data suggesting propagating aggregation in experimental animals [41], have led to the suggestion that α-Synuclein pathology may progress in a prion-like manner. However, the role of α-Synuclein in PD pathogenesis and its relationship to the physiological functions of the protein are currently unclear.

Mechanisms that link mitochondrial dysfunction and α-Synuclein in PD are incompletely resolved. Rats exposed systemically to the mitochondrial complex I inhibitor rotenone show widespread impairment of mitochondrial respiratory function, but relatively selective neuropathological abnormalities that replicate many features of sporadic PD. These include degeneration of substantia nigra dopaminergic neurons and their striatal projections and, importantly, accumulation of α-Synuclein immunoreactive inclusions resembling Lewy pathology in surviving cells [4,8,59]. We previously demonstrated that α-Synuclein knockdown in this model, using a viral vector to express a short hairpin RNA (shRNA) targeting the *Snca* mRNA transcript, ameliorated neurological and neuropathological phenotypes [76]. Animals with ≈30% decrease in α-Synuclein expression in substantia nigra dopaminergic neurons on one side showed maintenance of motor function in the contralateral limbs during rotenone exposure, even while limbs contralateral to the control side (with normal α-Synuclein expression) showed progressive parkinsonism. Pathologically, loss of dopaminergic neurons, their terminals and their dendritic arborization were mitigated significantly by decreased α-Synuclein expression. This establishes a critical role for α-Synuclein in the mechanisms mediating degeneration of nigral dopaminergic neurons secondary to mitochondrial dysfunction [76]. Interestingly, we further demonstrated that the earliest motor abnormalities in this model, occurring prior to the degeneration of nigral dopaminergic neurons and their striatal terminals, were also rescued by α-Synuclein knockdown [76]. These data strongly suggest that neuronal dysfunction preceding neurodegeneration underlies the initial motor abnormalities seen in the rat model, and that the relevant cellular mechanisms are α-Synuclein-dependent. The importance of these observations lies in their translational potential. An emerging concept considers the possibility that salvageable neurons with impaired health or function may contribute to the initial clinical presentation of PD [33]. In this context, mechanisms underlying interactions between α-Synuclein and mitochondria could provide therapeutic targets to mitigate cellular pathophysiology and prevent progression.

Chemical alterations of cellular components by reactive oxygen species likely underlies pathogenesis in the rotenone model of PD [4,58]. Oxidative damage is an attractive mechanism to explain the severe neuropathology in dopaminergic neurons in PD, since several properties inherent in their neurochemistry may cause or exacerbate oxidative stress. Dopamine is readily oxidized to a quinone, both generating ROS and becoming a reactive oxidant itself in the process [25,26]. In addition, catabolism of dopamine by MAO-B yields peroxide that can be converted to the highly-reactive hydroxyl radical in the presence of Fe^{2+}, an essential cofactor for tyrosine hydroxylase (the rate-limiting enzyme in dopamine biosynthesis). In this context, we hypothesized that the protection of dopaminergic neurons from rotenone by down-regulation of α-Synuclein may be attributable to decreased formation of superoxide or peroxide within mitochondria, or attenuated peroxide flux to other parts of the cell, thereby mitigating oxidative stress and damage. Here, we present data from complementary approaches in different model systems showing that α-Synuclein strongly influences redox biochemistry in dopaminergic neurons *in vivo*. We show that rotenone induces extensive thiol oxidation in rat substantia nigra dopaminergic neurons prior to their degeneration, and this is mitigated by α-Synuclein knockdown. We further demonstrate novel transgenic zebrafish models that allow, for the first time, dynamic real-time observation of cytoplasmic peroxide flux, and changes in glutathione redox potential, in dopaminergic neurons *in vivo*. Using these unique reagents, we show that α-Synuclein both (i) amplifies cytoplasmic peroxide flux following exposure to mitochondrial inhibitors and (ii) impairs cellular mechanisms for buffering redox perturbations.

2. Materials and methods

2.1. Ethical approval

All studies were carried out with approval from the University of Pittsburgh Institutional Animal Care and Use Committee, in accordance with the NIH *Guide for the Care and Use of Laboratory Animals*.

2.2. Viral vectors

An AAV2 vector, AAV-sh[Snca], was used to deliver a short hairpin RNA targeting the rat *Snca* transcript resulting in decreased α-Synuclein expression, together with a GFP reporter, as described in our previous work [75,76]. The shRNA is specific for α-Synuclein and does not alter expression of β- or γ-Synuclein. The control vector AAV-sh[Ctrl] is isogenic except for encoding a non-targeting control shRNA. Plasmids containing the vector genomes can be obtained from Addgene (#75438 and #75437). Vectors for this study were prepared to high titer and purity by plasmid co-transfection at the University of Pennsylvania Vector Core.

2.3. In vivo rat studies

Vector inoculations were carried out as described in our previous work [75,76]. Adult male Lewis rats (retired breeders; Charles Rivers, Wilmington, MA) were anesthetized with 3% isoflurane. 2 μL viral vector suspension was infused dorsal to the substantia nigra (−5.8 mm anterior/posterior, ±2.2 mm right/left, −7.5 mm ventral to bregma) using a Hamilton syringe with a 30-gauge needle (45° bevel) at a rate of 0.2 μL/min. AAV-sh[SNCA] (right) and AAV-sh[Ctrl] (left) were each infused at a concentration of 2.0×10^{12} GC/mL, giving a total dose 4.0×10^9 GC/side. Starting from 21 days after vector infusion, animals received daily intraperitoneal rotenone (2.8 mg/kg/d) dissolved in 2% DMSO, 98% Miglyol for 6 days as described previously [8,76]. Animals

were weighed daily and monitored for development of motor signs using a postural instability test, which is sensitive to disruption of contralateral nigrostriatal function [71]. Briefly, rats were suspended with one forepaw in contact with a textured surface and moved forward until a corrective forelimb placement was made. Following initial training, the displacement necessary to trigger forelimb movement was measured four times on each side of each animal during the six days of rotenone administration.

2.4. Immunohistology and RNA in situ hybridization analysis of rat brain samples

Rats were anesthetized deeply with pentobarbital (50 mg/kg) and perfused with PBS followed by 4% paraformaldehyde. Brains were then removed, post-fixed in 4% paraformaldehyde and cryoprotected in sucrose. Frozen brains were sectioned into 35 μm slices using a freezing-stage microtome. Effective shRNA targeting of the *Snca* transcript was verified by RNA *in situ* hybridization in representative midbrain sections from all animals. A digoxigenin-labeled cRNA probe to *Snca* was hybridized with tissue sections overnight at 42 °C, and bound probe detected using an alkaline phosphatase–conjugated *anti*-digoxigenin antibody (Roche) and a histochemical reaction using an AP substrate with a purple reaction product (BM Purple, Roche) as described in our previous work [75,76]. For confirmation of vector transduction, sections were preincubated with 3% H_2O_2 in PBS for 10 min followed by 10% normal donkey serum in PBS for 1 h, then incubated overnight at room temperature with primary antibody to GFP (#AB290, 1:4000, Millipore). Bound primary antibody was visualized using a biotinylated secondary antibody with avidin–biotin–peroxidase complexes (ABC; Vector Lab) followed by a histochemical reaction with 3,3-diaminobenzidine (DAB; peroxidase substrate kit SK-4100; Vector Lab) to yield a brown chromogenic product.

2.5. Thiol histochemistry

Thiol labeling and imaging were completed exactly as previously described [28]. Briefly, brains were fixed for 3 days in PBS, 4% paraformaldehyde, 1 mM *N*-ethylmaleimide, and 2 μM Alexa-680 maleimide (#A20344; Invitrogen), then cryoprotected in 30% sucrose for 5 days. Sections of 35 μm thickness were prepared using a microtome, washed 3 times in PBS and incubated in 5 mM TCEP in PBS for 30 min, followed by 1 mM *N*-ethylmaleimide and Alexa-555 maleimide (#A10258; Invitrogen) in PBS. Vector-transduced dopaminergic neurons were then labeled using antibodies to Tyrosine Hydroxylase (#AB152, 1:2000, Millipore) and GFP (#MAB3580, 1:4000, Millipore), with secondary antibodies conjugated to Alexa-405 and Alexa-488 respectively. Confocal microscopy was employed to image all four channels, using settings that avoided pixel saturation, and ratiometric images were generated from the disulfide and thiol channels. For quantification, regions of interest corresponding to transduced dopaminergic neurons (defined by immunoreactivity to TH and GFP) were defined manually by an observer blinded to the thiol channels. The mean disulfide:thiol ratio in each region of interest was then quantified for 100–150 substantia nigra neurons from 10 to 15 midbrain sections from each side of each brain. Similar methods were used in striatal sections, except the TH signal was used to define regions of interest corresponding to dopaminergic terminals.

2.6. Transgene constructs

hsa.SNCA-p2A-nls-mCherry and p2A-nls-mCherry: A PCR fragment containing p2A-nls was amplified from pTM-mCherry-2A-NLSeGFP (a gift from Dr. Michael Tsang, University of Pittsburgh, Pittsburgh, USA) using primers 5′-CGGGATCCGGAGCCACGAAC-3′ and 5′-CCATGTTATCCTCCTCGCCCTTGCTCAC-3′ and inserted into pmCherry (Clontech, Carlsbad, CA), yielding a plasmid template for amplification of p2A-nls-mCherry using primers 5′GTGATATCCGGAGCCACGAACTTC-3′ and 5′-CCGCTCGAGCCGCTACTTGTACAGC-3’. The resulting amplicon was digested with *Eco*RV/*Xho*I and inserted into the *Eco*RV/*Xho*I sites of pT2MUASMCS (a gift from Dr. Koichi Kawakami, National Institute of Genetics, Mishima, Japan) to generate pT2-5UAS-p2A-nls-mCherry. cDNA encoding human α-Synuclein was cloned from NT2 teratoma cells by RT-PCR and sequence-verified. A PCR fragment containing the ORF was then amplified from the resulting plasmid using primers 5′-GAAGATCTGTCGACGAATTCCC-3′ and 5′-CCGGCTTCAGGTTCGTAGTCTT-3′, *Bgl*II/*Eco*RV digested, and ligated into the *Bgl*II/*Eco*RV sites of pT2-5UAS-p2A-nls-mCherry to yield pT2-5UAS-hsa.SNCA-p2A-nls-mCherry. The sequences of both plasmids were confirmed by DNA sequencing. Transient co-transfection of HEK293T cells with these plasmids and a Gal4-encoding plasmid allowed confirmation of nuclear mCherry fluorescence by microscopy and expression of human α-Synuclein by Western blot.

roGFP2-Orp1: A PCR fragment containing roGFP2-Orp1 was amplified from pLPCX-roGFP2-Orp1 (a gift from Dr. Tobias Dick, German Cancer Research Center, Heidelberg, Germany) using primers 5′-CATGCCATGGTGAGCAAGGGCGAG-3′ and 5′-CCGCTCGAGCTATTC-CACCTCTTTCAAA-3′, *Nco*I/*Xho*I digested and inserted into the *Nco*I/*Xho*I sites of pT2MUASMCS to generate plasmid pT2-5UAS-roGFP2-Orp1. The plasmid was verified by DNA sequencing and roGFP2 expression confirmed by co-transfection of HEK293T cells with a plasmid encoding Gal4-VP16.

Grx1-roGFP2: A PCR fragment containing Grx1-roGFP2 was amplified from pQE-60-Grx1-roGFP2-His (a gift from Dr. Tobias Dick, German Cancer Research Center, Heidelberg, Germany) using primers 5′-CATGCCATGGCTCAAGAGTTTGTGA-3′ and 5′-AAGGCCTTACTTGTA-CAGCTCGTCCA-3′, *Nco*I/*Stu*I digested and inserted into the *Nco*I/*Eco*RV sites of pT2MUASMCS to generate plasmid pT2-5UAS-Grx1-roGFP2. Verification by DNA sequencing and roGFP2 expression *in vitro* was identical to pT2-5UAS-roGFP2-Orp1.

2.7. Transgenic zebrafish

Zebrafish larvae were generated by crossing adult WT (strain AB), *Casper* (genotype: *roy*$^{-/-}$; *nacre*$^{-/-}$) [69] and Tg(*otpb:gal4-vp16, myl7:gfp*)^{zc57} (referred to as Tg(*otpb:gal4*) for brevity) zebrafish [21]. Embryos were raised at 28.5 °C in cycles of 14 h light – 10 h dark, with illumination in white light at 200 Lux, color temperature 3700 K, in E3 buffer (5 mM NaCl, 0.17 mM KCl, 0.33 mM $CaCl_2$, 0.33 mM $MgSO_4$; all chemicals were supplied by Sigma, St. Louis, MO). Transgenic Tg(*UAS:hsa.SNCA-p2A-nls-mCherry*)^{Pt423}, Tg(*UAS:p2A-nls-mCherry*)^{Pt424}, Tg(*UAS:roGFP2-Orp1*)^{Pt428} and Tg(*UAS:Grx1-roGFP2*)^{Pt429} lines were generated using the Tol2 transposon method as in our previous work [73]. Embryos were injected at the 1-cell stage with 1 – 2 nL of transgene solution (25 μg/μL transgene plasmid; 0.5% phenol red; 240 mM KCl; 40 mM 4-(2-hydroxyethyl)-1-piperazineethanesulfonic acid, pH 7.4; 50 ng/μL *tol2* transposase mRNA; nuclease-free H_2O). Surviving embryos were raised to sexual maturity and mosaic F0 chimeras identified by expression of nls-mCherry or roGFP2 fluorescence (indicating transgene transmission) in the F1 progeny resulting from crossing with a Gal4 driver line. Transgenic lines were established from multiple F1 founders for each construct. The lines used in these studies were selected for robust transactivation of the transgene by Gal4, minimal variegation, and stable monoallelic Mendelian transgene inheritance over multiple generations.

2.8. Zebrafish chemical exposure

For dynamic imaging studies, MPP^+ or rotenone were added to the bath during the experiment at the indicated final concentrations. For prolonged exposure experiments, larval zebrafish were placed in E3 buffer containing MPP^+, rotenone, or no chemical at the indicated final concentrations at 3 dpf (single timepoint intravital imaging) or 4dpf

(motor function) and kept at 28.5 °C overnight in darkness for 16 h. Larvae were then washed in fresh E3 buffer and allowed to recover in E3 at 28.5 °C in white light for 1 h prior to further analysis.

2.9. Zebrafish motor function

Zebrafish locomotor behavioral testing was performed exactly as described in our previous work [73,77]. 5dpf zebrafish larvae were placed in the wells of a black-walled 96-well plate with an optical glass bottom in an incubator at 28.5 °C. The wells were illuminated from above using an infrared light source and the movements of back-illuminated zebrafish larvae were imaged from below using an infrared-sensitive video camera and IR-pass filter. After acclimatization, responses were elicited to 3 cycles of alternating 10min darkness followed by 10min light (200 Lux, white light, color temperature 3500 K). Video recordings were analyzed offline using the open-source zebrafish neurobehavioral applications *LSRtrack* and *LSRanalyze* [9].

2.10. Immunofluorescence of zebrafish brain

Zebrafish were anesthetized in tricaine and fixed in 4% PFA at 4 °C for 16hr, then rinsed with cold PBS prior to preparation of frozen sections or dissection to remove the brain for whole-mount analysis. Sections were labeled for immunofluorescence as described previously [73] using primary antibodies to TH (#MAB318, 1:500, Millipore) and human α-Synuclein (#sc7011 R, 1:400, Santa Cruz). Whole mount immunofluorescence labeling was carried out as described previously [18], using primary antibodies to TH (rabbit polyclonal, Millipore, # AB152; 1:1000) and GFP (chicken polyclonal, Abcam, Cat # AB13970; 1:5000). Brains were then washed in PBS and passed through a glycerol series to 70% for imaging.

2.11. Western blot of zebrafish brain

Head/brain regions from 4dpf Ctrl and α-Syn zebrafish (n = 24 larvae per group) were micro-dissected and pooled samples were extracted with RIPA buffer. Proteins were separated using a 15% SDS-PAGE gel, then transferred to a nitrocellulose membrane (Li-COR #926–31092). After blocking, human α-Synuclein was detected using a mouse monoclonal antibody (BD #610787; 1:500) and zebrafish β-Actin using a rabbit polyclonal antibody (Sigma #A2066; 1:4000), incubated simultaneously at 4 °C overnight. Following washing and detection of bound antibody using nIR fluorophore-conjugated secondary antibodies (IRD680 goat anti-mouse, 1:10,000, LI-COR, 926–68070; IRD800 goat anti-rabbit, 1:10,000, Li-COR, #926–32211) the blot was imaged using a Li-COR Odyssey scanner.

2.12. Intravital imaging of roGFP2 biosensors

Transgenic zebrafish larvae were anesthetized in 0.015% tricaine and immobilized in a 35 mm glass bottom dish (MatTek, Ashland, MA), in a custom mounting device (supplemental figure 1). The dorsum of the head was in contact with the glass of the dish and the tail portion of the larvae embedded in agarose to prevent movement while the head and mouth were directly in contact with the medium in the bath to allow chemical exposures. Images were acquired using a Nikon A1 inverted confocal laser point scanning microscope equipped with Nikon Perfect Focus System and a 20× long working-distance water immersion objective (NA = 0.95; #MRD77200, Nikon, Melville, NY). For dynamic time-lapse image series, Z-plane image stacks extending through the diencephalon were acquired every 3–4 min over 4–11 h as indicated in each figure. Emission at 515 nm was detected after sequential excitation at 405 nm and then 488 nm. Excitation laser intensities and detector sensitivity settings were identical throughout replicate experiments for each dataset.

2.13. Image processing and ratiometric analysis

Ratiometric analyses, including generation of ratiometric color maps and quantitative analyses were carried out using NIS-Elements software (Nikon, Melville, NY). All images first underwent deconvolution using a blind, iterative photon reassignment approach that ensured that the quantitative features of the data set were maintained. Time-lapse image series were then aligned spatially over time. For 3D analyses, individual neurons in binarized images were identified in confocal image Z-stacks using unbiased automated spot detection. For time-lapse image series, neuronal volumes of interest were tracked over time, and those identified over the entire recording were analyzed for time course experiments. For each neuron at each time point, the mean ratio [515 nm emission following 405 nm excitation]/[515 nm emission following 488 nm excitation] within the defined volume of interest was calculated to produce a single data point per cell and time point. Cells from replicate experiments in multiple zebrafish were analyzed for each figure. For single time point imaging, the methodology was identical, with the exception that the tracking step was eliminated and all neurons identified by the spot detection algorithm were included in analysis. For 2D analyses, ratiometric images were generated for each plane of the Z-stack, then maximal intensity projections made to reduce the ratiometric image stack to 2 dimensions. Regions of interest corresponding to neurons in each group were then defined in the 2D ratiometric images and histograms of the binned frequency distribution generated. Similar results were obtained from analyzing single image planes or generating extended depth focus (EDF) images from the Z-stack instead of maximal intensity projection images.

2.14. Statistical analysis

Experiments were powered to detect >15% differences between treatment conditions with $\alpha = 0.05$ and $\beta = 0.8$, using expected effect sizes and variances estimated from pilot studies and published data. For experiments in rats where comparisons were made between the two sides of each animal, statistical analyses were carried out using 2-tailed paired t-tests. For time course data, analysis was carried out using 2-way repeated measures ANOVA with time and experimental group as variables, using Šidák's multiple comparisons test to compare experimental groups at each time point. For comparison of baseline and post-exposure data in two groups, 2-way ANOVA with chemical exposure and experimental group as variables was combined with Tukey's multiple comparisons test to compare groups. For experiments in which four different groups of zebrafish were compared, analysis was carried out using 1-way ANOVA with Tukey's multiple comparisons test to compare groups.

3. Results

3.1. α-Synuclein promotes neuronal oxidative stress in the rat rotenone model of sporadic Parkinson's disease

In view of prior data suggesting that oxidative stress is a primary mechanism underlying neurodegeneration in the rotenone model [58], we tested the hypothesis that rescue of neurological function by α-Synuclein knockdown is attributable to prevention of cellular oxidative damage.

Rats received AAV-sh[Snca] into the right substantia nigra and AAV-sh[Ctrl] (an isogenic control vector that expresses a non-targeting shRNA) into the left substantia nigra. After 21 days of recovery from surgery, during which animals were trained to participate in motor testing, rotenone dissolved in vehicle, or vehicle only (n = 6 per group), were delivered by intraperitoneal injection daily for 6 days (Fig. 1A). Exposure to rotenone in this way caused modest weight loss as previously reported [76] (Fig. 1B). Forelimb motor function was evaluated during the 6 days of rotenone exposure, using a postural instability test to determine the body displacement necessary to provoke corrective

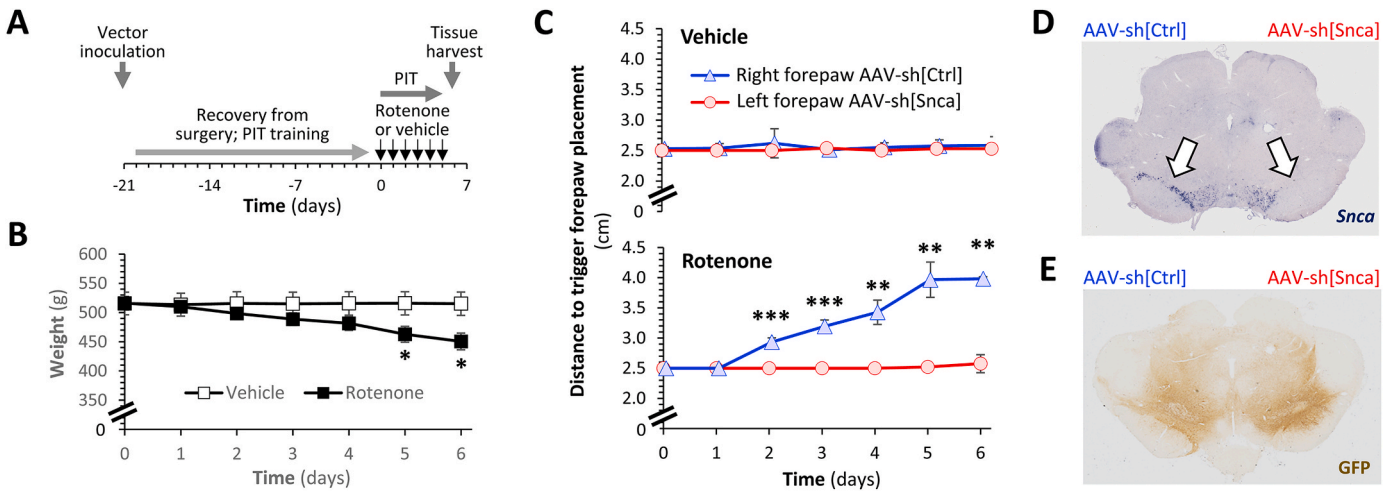

Fig. 1. α-Synuclein knockdown prevents rotenone-induced loss of dopaminergic function *in vivo*.
A: Schematic depiction of the experimental sequence for the rat studies shown in panels B–E and in Fig. 2.
B: Mean ± SE weight of rats treated with vehicle (white squares) or rotenone (2.8 mg/kg/day; black squares) by intraperitoneal injection over 6 consecutive days. $p <$ *0.05 vehicle versus rotenone, 2-way repeated measures ANOVA with Šidák multiple comparisons test.
C: Mean ± SE distance to trigger a corrective forelimb movement during postural instability tests in rats treated with vehicle (upper panel) or rotenone (lower panel). In each case, data are shown separately for the left forelimb (red; opposite to right hemisphere that received AAV-sh[Snca]) and right forelimb (blue; opposite the left hemisphere that received AAV-sh[Ctrl]). $p <$ **0.01, **0.001, left *vs.* right, 2-way repeated measures ANOVA with Šidák multiple comparisons test.
D, E: Micrographs showing midbrain sections from a vehicle-treated rat, labeled using (D) RNA *in situ* hybridization to detect the *Snca* mRNA transcript (purple) or (E) immunohistochemistry to detect expression of GFP (brown). Arrows in the upper panel indicate the substantia nigra. The side of the brain that received each vector is marked above the sections.

forelimb movements. This yields a quantitative measurement of motor function on each side that is dependent on nigrostriatal dopaminergic function in the contralateral hemisphere [71]. In animals that received vehicle only, no baseline asymmetry or progressive changes in motor function attributable to α-Synuclein knockdown were noted, in keeping with our prior work [75,76]. In contrast, a progressive increase in the distance necessary to trigger a corrective movement was noted in the right forelimbs (contralateral to AAV-sh[Ctrl] transduction) of rats that received rotenone, whereas the left forelimbs of the same animals (contralateral to AAV-sh[Snca] transduction) showed no changes in motor function during rotenone exposure and continued to show similar trigger distances to animals that received vehicle only (baseline: left 2.50 ± 0, right 2.50 ± 0 mm; rotenone day 6: left 2.58 ± 0.08, right 3.98 ± 0.02 mm; $p = 0.0014$, left *vs.* right day 6, 2-way repeated measures ANOVA with Šidák multiple comparisons test; Fig. 1C). Animals were sacrificed following motor testing at day 6. Loss of the *Snca* mRNA transcript on the AAV-sh[Snca] side of the brain was confirmed by RNA *in situ* hybridization (Fig. 1D) and viral transduction of midbrain neurons on both sides was confirmed by immunohistochemistry for the GFP reporter gene expressed by both vectors (Fig. 1E). Decreased α-Synuclein expression has been shown in the rat substantia nigra following loss of the *Snca* mRNA in our previous studies using this vector [75,76]. Together, these data confirm that α-Synuclein knockdown protected the function of nigral dopaminergic neurons exposed to rotenone in this cohort of rats.

We next evaluated oxidative stress in the substantia nigra dopaminergic neurons of these animals using a histochemical method (depicted schematically in Fig. 2A) in which reduced and oxidized thiols are labeled with separate fluorophores [28]. Confocal imaging of the two channels allows construction of a ratiometric map showing relative regional quantification of thiol oxidation throughout a tissue section. Sections were also labeled for tyrosine hydroxylase (TH) and GFP in separate channels, so that the mean pixel-by-pixel ratio of oxidized/reduced thiol signal could be quantified within 80–120 dopaminergic neurons on each side of the midbrain in each animal. Signal attributable to both reduced and oxidized thiols was detectable in the substantia nigra on both sides of vehicle-treated rats, although the oxidized thiol signal was weaker. In some of the vehicle-treated rats, the oxidized/reduced thiol ratio was significantly lower in dopaminergic neurons on the side that received AAV-sh[Snca] than the control side, although this was not observed in every animal and the trend was not statistically significant for the group as a whole (control side 0.61 ± 0.09 *vs.* α-Synuclein knockdown side 0.46 ± 0.19; $p = 0.12$, 2-tailed paired *t*-test; Fig. 2D). In animals that received rotenone, a large increase in the oxidized thiol signal was readily apparent in the AAV-sh[Ctrl]-transduced substantia nigra, but not on the AAV-sh[Snca] side (Fig. 2B). This was reflected in a large rotenone-dependent rightwards shift in the pixel-by-pixel ratiometric histogram for dopaminergic neurons from the control side compared with the α-Synuclein knockdown side of the same midbrain sections (example shown in Fig. 2C). Within each of the individual rats that received rotenone, there was a robust and statistically significant increase in thiol oxidation within dopaminergic neurons on the control side of the brain compared with the α-Synuclein knockdown side (Fig. 2D). Overall, for the entire group, the mean oxidized/reduced thiol ratio within dopaminergic neurons was significantly higher on the AAV-sh[Ctrl] side than the AAV-sh[Snca] side in the same sections (control 3.69 ± 0.76 *vs.* α-Synuclein knockdown 1.06 ± 0.24; $p = 0.004$, 2-tailed paired *t*-test; Fig. 2E). Similar findings were observed in the striatum (supplemental figure 2), where the AAV-sh[Snca] side of rats exposed to rotenone showed a significantly lower ratio of oxidized to reduced thiols than the AAV-sh[Ctrl] side, whereas no such asymmetry was apparent in vehicle-treated animals.

Together, these data show that protection of dopaminergic neuronal function by α-Synuclein knockdown correlates with a dramatic attenuation in thiol oxidation within the cell body and synaptic terminals of these neurons during rotenone exposure.

3.2. *Transgenic zebrafish expressing human α-Synuclein and a peroxide biosensor in dopaminergic neurons*

Pathology in the rotenone model is relatively selective for the PD-vulnerable substantia nigra [4,8], suggesting that mechanisms mediating pathogenesis might be most prominent within dopaminergic neurons *in vivo*. Dynamic measurements of reactive oxygen species and

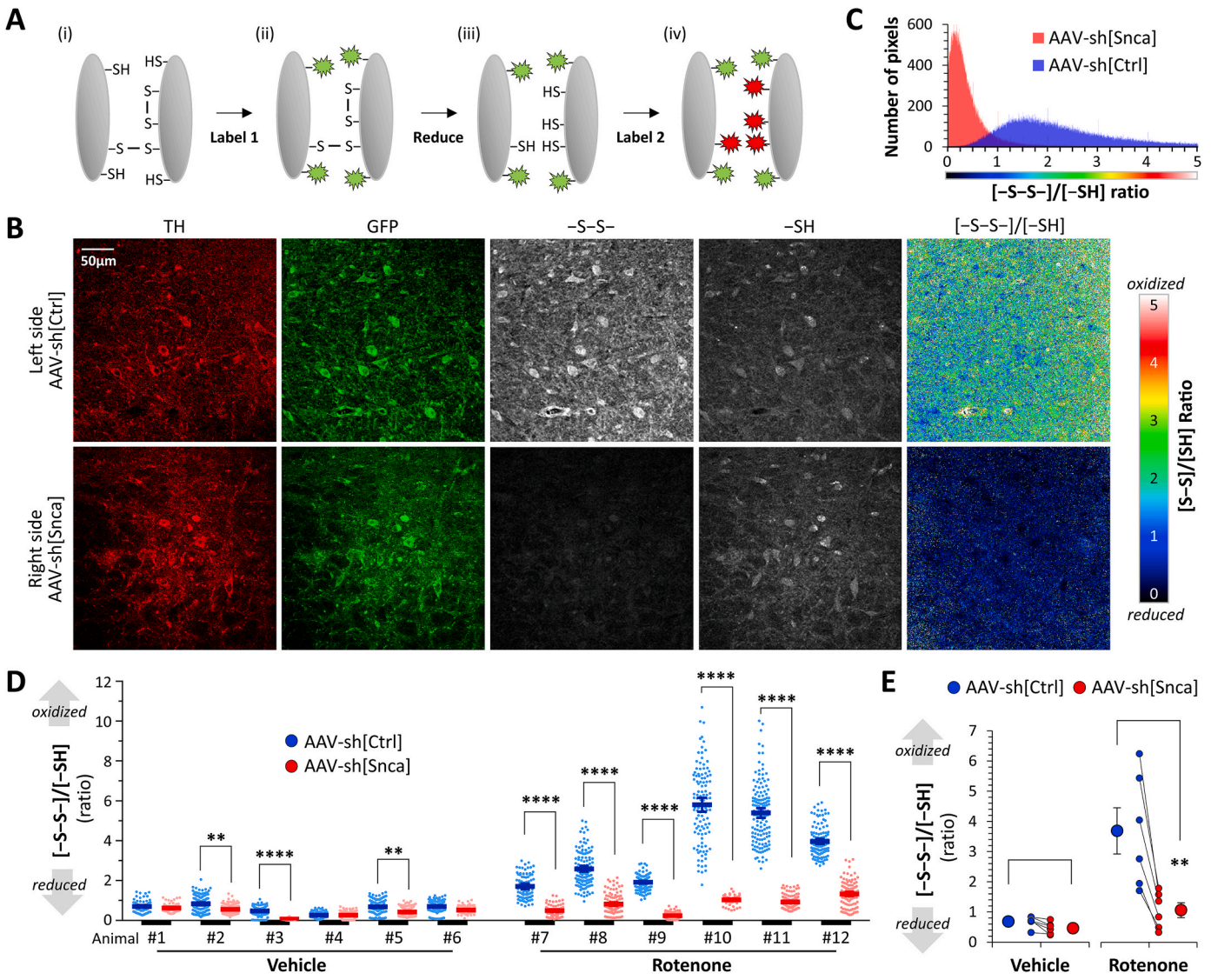

Fig. 2. α-Synuclein knockdown mitigates rotenone-induced thiol oxidation in dopaminergic neurons *in vivo*.
A: Schematic illustration of the thiol histochemical method used in panels B–E. Reduced thiol groups were irreversibly labeled with a maleimide-conjugate fluorophore. Disulfide bonds were then reduced and the resulting newly-generated thiols labeled with maleimide conjugated to a second fluorophore. The relative signal intensity of the two fluorophores was determined by confocal microscopy, providing a map of thiol oxidation in the tissue sample.
B: Confocal micrographs of a midbrain section from a rat that received AAV-sh[Ctrl] in the left substantia nigra (top row) and AAV-sh[Snca] in the right substantial nigra (bottom row), followed by 6 days of rotenone (see Fig. 1A). The images show: immunofluorescence for tyrosine hydroxylase (TH; red); immunofluorescence for GFP (green); oxidized thiols (-S-S-; grayscale); reduced thiols (-SH; grayscale). The final column shows the ratiometric image for oxidized/reduced thiols, pseudo-colored according to the scale shown to the right of the panel.
C: Histogram showing the frequency distribution of the oxidized/reduced thiol ratio in each pixel of the images shown in panel B.
D: Scatterplots showing thiol oxidation, analyzed in dopaminergic neurons on both the left (AAV-sh[Ctrl]; blue) and right (AAV-sh[Snca]; red) sides of the substantia nigra in 6 vehicle (animals #1 - #6) and 6 rotenone (animals #7 - #12) treated rats. Data points show the mean oxidized/reduced thiol ratio in individual dopaminergic neurons, bars show mean ± SE for each side of each animal. $p <$ **0.01, ****0.0001, left *vs.* right, 1-way ANOVA with Tukey multiple comparisons test.
E: Mean dopaminergic neuron thiol oxidation is shown for the two sides of the midbrain in each animal (small markers; the two sides of each animal are connected by a line) alongside mean ± SE for all six animals in each group (large markers). $p < 0.01$**, left *vs.* right, 2-tailed paired *t*-test.

cellular oxidative stress are not yet possible in the substantia nigra of living rats. Consequently, in order to further delineate mechanisms underlying α-Synuclein-dependent thiol oxidation in dopaminergic neurons, we took advantage of the ability to carry out intravital imaging of genetically-encoded biosensors in the intact CNS of a transparent zebrafish model.

Zebrafish express β-Synuclein and dual γ-Synuclein paralogues, but lack a gene expressing α-Synuclein [44,64]. In order to examine the role of human α-Synuclein in redox biology *in vivo*, we first generated transgenic zebrafish expressing the human SNCA gene in ventral diencephalic dopaminergic neurons that are thought to be the anatomical homologue of the mammalian nigrostriatal system [54]. Tg(*UAS:hsa.SNCA-2A-nls-mCherry*) zebrafish were constructed to express human WT α-Synuclein and a nuclear-localized mCherry reporter as separate proteins from the same transgene-derived mRNA, using a self-cleaving viral 2A peptide [51] (Fig. 3A). The mCherry reporter allows identification of cells expressing α-Synuclein by non-invasive epifluorescence microscopy. A control line Tg(*UAS:2A-nls-mCherry*) is isogenic but does not express α-Synuclein. Transgene expression from the UAS enhancer in both lines was activated by crossing with a Gal4 driver line, Tg(*otpb:gal4*), which is expressed within DC4 – 6 diencephalic dopaminergic neurons and an adjacent group of non-dopaminergic neurons for

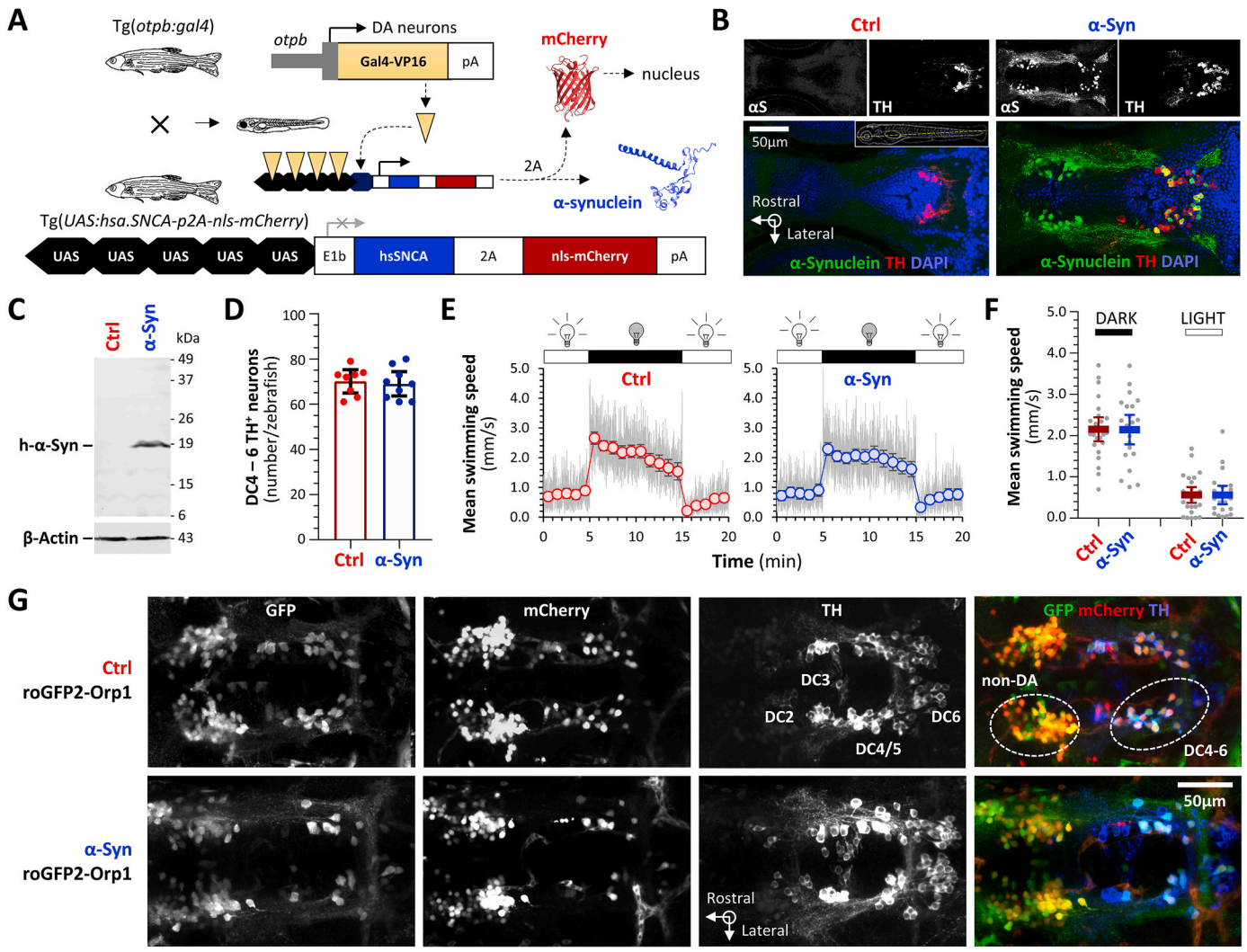

Fig. 3. Transgenic zebrafish expressing human α-Synuclein and a ratiometric biosensor of cytoplasmic peroxide in dopaminergic neurons *in vivo*.
A: Schematic depiction of the transgene constructs and breeding scheme used to express human α-Synuclein in ventral diencephalic dopaminergic neurons of larval zebrafish. For brevity, *roy*$^{-/-}$; *nacre*$^{-/-}$; Tg(*optb:gal4*); Tg(*UAS:hsa.SNCA-p2A-nls-mCherry*) larvae, which express human α-Synuclein and nuclear-localized mCherry as separate proteins on a transparent genetic background lacking pigment, are referred to as "α-Syn" zebrafish. Control *roy*$^{-/-}$; *nacre*$^{-/-}$; Tg(*optb:gal4*); Tg(*UAS:nls-mCherry*) larvae, which lack an α-Synuclein transgene from the UAS responder cassette but are otherwise isogenic, are referred to as "Ctrl" zebrafish.
B: Confocal single-plane images of histological sections from the diencephalon of Ctrl (left) and α-Syn (right) zebrafish, labeled by immunofluorescence for human α-Synuclein (αS) and tyrosine hydroxylase (TH). The pseudocolored overlaid images are shown with a nuclear counter label (α-Synuclein, green; TH, red; DAPI, blue). The plane of the sections is shown by the dotted yellow line in the inset panel for the Ctrl sample.
C: Western blot of pooled head region lysates from Ctrl (left lane) and α-Syn (right lane; n = 24 larvae per lane) zebrafish, probed with an antibody to human α-Synuclein (upper panel) and β-Actin as a loading control (lower panel). The positions of molecular weight markers are shown to the right of the blot image.
D: Exhaustive counts of TH-expressing dopaminergic neurons in diencephalic groups DC4 – 6 from Ctrl (red; n = 8) and α-Syn (blue; n = 9) larvae at 5dpf. Data points show values from single zebrafish; bars show mean ± SE. There was no significant difference between Ctrl and α-Syn zebrafish.
E: Swimming movements of Ctrl (red, left graph) and α-Syn (blue, right graph; n = 24 each group) larvae at 5dpf were recorded by infrared videography (4 frames/s) in response to cycles of 10 min bright ambient light (white, 200 Lux) followed by 10 min darkness (visual motor response, VMR; ambient illumination is indicated above each graph). Video tracking software was used to quantify larval displacements at frame transitions and responses were averaged over 3 light-dark cycles. The grey traces show mean frame-to-frame displacements scaled to represent mean instantaneous swimming speed in mm.s^{-1}. The markers and bars show mean swimming speed ± SE for each 1-min time bin.
F: Scatter plots showing mean swimming speed during the dark (left) and light (right) phases of the VMR for each zebrafish. Bars show mean ± SE (n = 24 larvae per group). Although there were robust responses to changes in illumination, there were no significant differences between Ctrl and α-Syn zebrafish.
G: Confocal z-plane projections of the diencephalic region of fixed, whole mount Ctrl; roGFP2-Orp1 (upper row) and α-Syn; roGFP2-Orp1 (lower row) zebrafish labeled with antibodies to GFP, mCherry and tyrosine hydroxylase. The overlaid images are shown in the right column (GFP, green; mCherry, red; TH, blue). Groups of TH-expressing diencephalic dopaminergic neurons that also express the *otpb* enhancer element used in the driver line are numbered in the Ctrl TH image. The Ctrl overlay image indicates the locations of the DC 4–6 dopaminergic neurons imaged in live zebrafish in Figs. 4–10 and a more rostral group of non-dopaminergic (non-DA) neurons that also expresses the *otpb* enhancer and was imaged for comparison.

comparison [21]. For brevity in subsequent sections, Tg(*otpb:gal4*); Tg(*UAS:hsa.SNCA-2A-nls-mCherry*) zebrafish that express human α-Synuclein and mCherry are referred to as 'α-Syn', and Tg(*otpb:gal4*); Tg(*UAS:2A-nls-mCherry*) zebrafish that express only mCherry are referred to as 'Ctrl'.

Immunofluorescence showed expression of human α-Synuclein in the cytoplasm, axons, and processes of both TH-expressing DC4 – 6 dopaminergic neurons and a more rostral group of non-dopaminergic

neurons, in α-Syn but not Ctrl zebrafish (Fig. 3B). Western blot analysis showed a single human α-Synuclein-immunoreactive band, migrating just below the 19 kDa marker in protein lysates from α-Syn but not Ctrl zebrafish brains (Fig. 3C). These data confirm expression of full-length human α-Synuclein in transgenic α-Syn zebrafish and indicate that the nls-mCherry reporter was separated efficiently from α-Synuclein by cleavage of the 2A peptide.

There were no baseline differences in the number of diencephalic DC4 – 6 dopaminergic neurons (Fig. 3D, supplemental figure 5C) in α-Syn versus Ctrl zebrafish (Ctrl 70.1 ± 2.1, α-Syn 69.0 ± 2.3 neurons/zebrafish, p = 0.73, unpaired *t*-test), showing that human α-Synuclein expression at the levels present in this transgenic line did not cause degeneration of dopaminergic neurons at timepoints up to 5 days post-fertilization (dpf). Likewise, there were no baseline differences in the spontaneous activity or locomotor responses to changes in ambient light between α-Syn and Ctrl zebrafish (Fig. 3E and F) showing that the function of dopaminergic neurons [20,35] was not impaired by human α-Synuclein expression at these levels (mean swimming speed in dark: Ctrl 2.16 ± 0.14, α-Syn 2.15 ± 0.17 mm s^{-1}, $p = 0.97$; mean swimming speed in light: Ctrl 0.56 ± 0.09, α-Syn 0.56 ± 0.11 mm s^{-1}, $p = 0.98$; unpaired 2-tailed *t*-tests). The absence of overt spontaneous phenotypes suggests that α-Syn zebrafish provide a suitable model to study the role of α-Synuclein in the proximate biochemical responses of dopaminergic neurons to mitochondrial inhibitors.

We next developed transgenic zebrafish expressing a ratiometric H_2O_2 biosensor, roGFP2-Orp1 [23]. Orp1 is a peroxidase that becomes oxidized during its reaction with H_2O_2; the proximity of Orp1 to roGFP2 in the fusion protein forms an efficient redox relay so that oxidized Orp1 causes rapid formation of a disulfide bond within the roGFP2 fluorophore by thiol-disulfide exchange. roGFP2 has dual excitation peaks at 405 nm and 488 nm. In its reduced form, maximal excitation occurs at 488 nm, whereas formation of a disulfide bond within the fluorophore causes a relative increase in excitation at 405 nm and decrease in excitation at 488 nm [23,43]. Consequently, the ratio of fluorescence emission intensity following excitation at each these two wavelengths (referred to as the 'roGFP2-Orp1 405/488 ratio' for brevity) is dependent on the amount of roGFP2 oxidation, which in the context of the irreversible peroxidase reaction mediated by Orp1 provides a

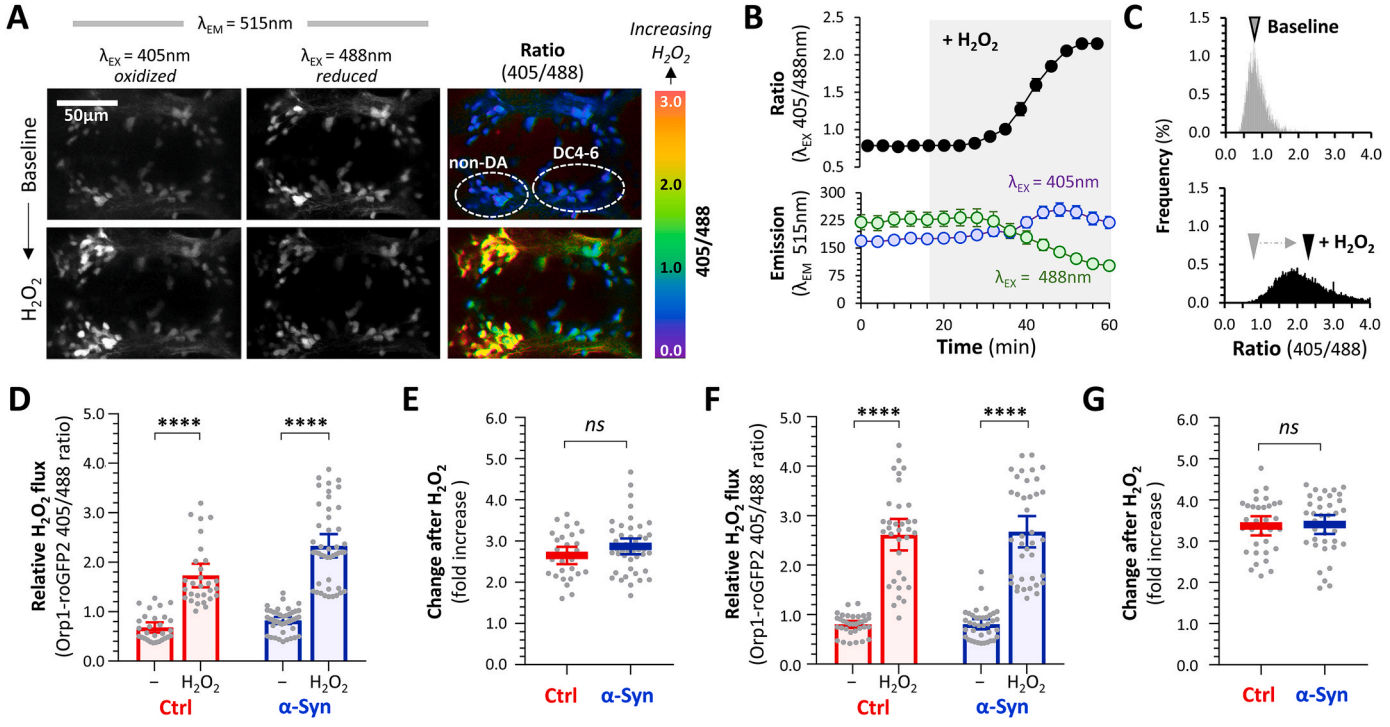

Fig. 4. Dynamic measurement of cytoplasmic H_2O_2 flux in dopaminergic neurons *in vivo*.

A: Intravital confocal microscopy was used to image the roGFP2-Orp1 biosensor in the ventral diencephalon of a live α-Syn; roGFP2-Orp1 zebrafish. Emission was captured at 515 nm following serial excitation at 405 nm (left column) and 488 nm (center column). The ratiometric image (right column; color scale shown to the right), calculated by dividing each image plane of the 405 nm dataset by the corresponding 488 nm image plane, shows relative integrated H_2O_2 flux. The positions of dopaminergic DC4 – 6 and adjacent non-dopaminergic neuronal groups are shown. The top row of images shows baseline steady-state images after equilibration in the imaging apparatus; the bottom row shows images of the same zebrafish after application of 3 mM H_2O_2 to the bath.

B: Unbiased 3D spot detection was used to define regions corresponding to cells within the DC4 – 6 cluster. Within each cell, mean emission following excitation at 405 nm or 488 nm (bottom graph) and the 405/488 ratio (top graph) was calculated in serial images acquired every 4 min for 1 h. Each datapoint shows mean ± SE (n = 9 neurons). After stable baseline data were collected, H_2O_2 was added to the bath at t = 18 min (shaded area).

C: Ratiometric histograms showing the frequency distribution of the roGFP2-Orp1 405/488 ratio from every pixel within areas corresponding to DC4 – 6 dopaminergic neurons in 2D images, at baseline (top panel) and after addition of H_2O_2 to the bath (bottom panel). The arrowhead shows the mean of each distribution.

D: Scatterplots showing baseline and peak roGFP2-Orp1 405/488 ratio, calculated using the 3D method, in DC4 – 6 dopaminergic neurons following exposure to H_2O_2. Data points represent individual neurons (Ctrl n = 29; α-Syn n = 45 neurons, combined from 4 replicate zebrafish); bars show mean ± SE; $p < 0.0001$****, 2-way ANOVA with Tukey multiple comparisons test.

E: Scatterplot showing fold increase in roGFP2-Orp1 405/488 ratio between baseline and post-H_2O_2 peak for each individual cell from panel D. Bars show mean ± SE; $p = 0.12$, 2-tailed unpaired *t*-test.

F: Baseline and peak roGFP2-Orp1 405/488 ratio in non-dopaminergic diencephalic neurons following exposure to H_2O_2. Data points, bars, and analysis identical to panel D (Ctrl n = 34; α-Syn n = 38 neurons).

G: Fold increase in roGFP2-Orp1 405/488 ratio between baseline and post-H_2O_2 is shown for each individual cell from panel F. Bars show mean ± SE; $p = 0.54$, 2-tailed unpaired *t*-test.

near-stoichiometric and integrative measure of cytoplasmic H_2O_2 flux [23,43]. Stable transgenic Tg(*UAS:roGFP2-Orp1*) zebrafish were generated on the *Casper* (*roy*$^{-/-}$; *nacre*$^{-/-}$) background that lacks pigment formation to facilitate intravital CNS imaging [69], and then crossed with Ctrl and α-Syn zebrafish that had also been bred onto the *Casper* background. This yielded transparent zebrafish expressing roGFP2-Orp1 and nls-mCherry within diencephalic dopaminergic neurons in the presence or absence of human α-Synuclein. Whole-mount immunofluorescence for GFP, mCherry and TH confirmed expression of both transgenes within the dopaminergic DC4 – 6 and more rostral non-dopaminergic diencephalic neurons that express Gal4 in the Tg (*otpb:gal4*) driver line (Fig. 3G) [21].

3.3. Detection of cytoplasmic peroxide in dopaminergic neurons in vivo

We next confirmed that the roGFP2-Orp1 biosensor could report dynamic H_2O_2 flux in the CNS of live Ctrl; roGFP2-Orp1 and α-Syn; roGFP2-Orp1 zebrafish *in vivo*. Larvae at 4 dpf were mounted in a glass-bottom dish (supplemental figure 1) and the ventral diencephalon was imaged in multiple planes by time-lapse confocal microscopy before and during exposure to exogenous H_2O_2. Emissions at 515 nm were collected following sequential excitation at 405 nm and 488 nm. Addition of H_2O_2 to the bath caused increased fluorescence emission following 405 nm excitation, and decreased fluorescence emission following 488 nm excitation, corresponding to oxidation of roGFP2 (Fig. 4). These changes were apparent in images from the separate excitation channels and clearly illustrated by colormaps of the roGFP2-Orp1 405/488 ratio (Fig. 4A). We developed two complementary workflows to quantify this ratiometric signal within dopaminergic and non-dopaminergic neurons (supplemental figures 3 and 4). First, we used unbiased 3D spot detection to determine the signal from each channel and the roGFP2-Orp1 405/488 ratio in volumetric regions corresponding to individual neurons. Using this method, the mean signal in each channel and 405/488 ratio for the neurons of a single zebrafish clearly illustrated the time course of the changes in roGFP2-Orp1 oxidation following H_2O_2 exposure (Fig. 4B). Second, we analyzed the roGFP2-Orp1 405/488 ratio in each pixel individually from 2D projections of the image stack. The distributions of these ratiometric data showed a robust rightwards shift following H_2O_2 exposure (Fig. 4C). Overall, the two analytic methods yielded very similar trends, supporting the validity of these strategies for quantification.

Using this approach, we quantified baseline and post-H_2O_2 roGFP2-Orp1 405/488 ratio as a measure of cytoplasmic H_2O_2 flux in dopaminergic DC4 – 6 (Fig. 4D and E) and non-dopaminergic (Fig. 4F and G) neurons of Ctrl and α-Syn zebrafish. There were no significant differences in baseline cytoplasmic H_2O_2 flux between Ctrl and α-Syn zebrafish, in either neuronal population (DA neurons: Ctrl 0.68 ± 0.05, α-Syn 0.78 ± 0.04, $p = 0.67$; non-DA neurons: Ctrl 0.80 ± 0.04, α-Syn 0.81 ± 0.05, $p = 0.99$; 2-way ANOVA with Tukey *post hoc* test). Following application of H_2O_2, both dopaminergic neurons (Ctrl 1.73 ± 0.12; α-Syn 2.33 ± 0.12) and non-dopaminergic neurons (Ctrl 2.62 ± 0.16; α-Syn 2.68 ± 0.16) showed substantial increases in roGFP2 oxidation ($p < 10^{-15}$ versus baseline for all four groups, 2-way ANOVA with Tukey multiple comparisons test). To compare the magnitudes of the responses between Ctrl and α-Syn zebrafish, we quantified the fold increase in ratiometric signal between baseline and post-H_2O_2 for each individual neuron (Fig. 4E, G). The responses of both Ctrl and α-Syn zebrafish to H_2O_2 were identical, showing that the biosensor functions similarly in both transgenic lines (fold increase in Orp1-roGFP2 405/488 ratio following H_2O_2: dopaminergic neurons, Ctrl 2.65 ± 0.10, α-Syn 2.87 ± 0.09, $p = 0.12$; non-dopaminergic neurons, Ctrl 3.30 ± 0.14, α-Syn 3.41 ± 0.11, $p = 0.54$; 2-tailed unpaired *t*-tests). These data demonstrate that: (i) relative cytoplasmic H_2O_2 flux can be quantified dynamically in CNS neurons *in vivo*; and (ii) the roGFP2-Orp1 biosensor behaves similarly in dopaminergic and non-dopaminergic neurons of both Ctrl and α-Syn zebrafish, and can therefore be deployed to compare their responses to mitochondrial inhibitors.

3.4. α-Synuclein augments cytoplasmic H_2O_2 flux in DA neurons in vivo following acute exposure to complex I inhibitors

We next interrogated the role of α-Synuclein in cytoplasmic peroxide flux in DA and non-DA neurons following acute exposure to MPP^+, a mitochondrial complex I inhibitor that is taken up specifically into dopaminergic neurons [30] and has been implicated in human parkinsonism [36]. In prior work, MPP^+ has been used extensively to model parkinsonism in larval zebrafish, and is significantly less toxic to zebrafish than rotenone, which causes lethality at very low concentrations (reviewed in Ref. [2]). Ctrl; roGFP2-Orp1 and α-Syn; roGFP2-Orp1 zebrafish were mounted adjacent to one another for intravital microscopy to ensure identical experimental conditions for direct comparison. Sequential images were acquired in tandem every 3–4 min for both genotypes, at baseline and following addition of MPP^+ to the bath. Images from the same zebrafish at baseline and 280 min post-MPP^+ are shown in Fig. 5A, illustrating increased oxidized roGFP2 and decreased reduced roGFP2 (indicating enhanced H_2O_2 flux) following MPP^+ exposure, only within α-Synuclein-expressing dopaminergic neurons. These changes were clearly apparent in the corresponding ratiometric images (Fig. 5A) and further illustrated in the pixel-wise ratiometric histograms (Fig. 5D). The roGFP2-Orp1 405/488 ratio was measured in sequential images throughout the experiment, using the 3D cell-based method (Fig. 5B and C). There was no baseline difference between Ctrl and α-Syn zebrafish. However, by ≈ 3.5 h after addition of MPP^+ to the water, the roGFP2-Orp1 405/488 ratio in the dopaminergic neurons of α-Syn, but not Ctrl, zebrafish increased progressively so that the curves diverged significantly by 4 h post-MPP^+ and were widely separated by the end of the experiment (Fig. 5B). Quantification of 55–60 neurons in each group from four replicate experiments confirmed there were no significant baseline differences in roGFP2-Orp1 405/488 ratio in the dopaminergic neurons of Ctrl versus α-Syn zebrafish (Ctrl 0.92 ± 0.04, α-Syn 0.95 ± 0.04, $p = 0.99$; 2-way ANOVA with Tukey multiple comparisons test; Fig. 5E) suggesting similar levels of basal cytoplasmic H_2O_2 flux regardless of α-Synuclein expression. Under these conditions, MPP^+ caused a modest increase in roGFP2-Orp1 405/488 ratio in the dopaminergic neurons of Ctrl zebrafish, which was not statistically significant (Ctrl post-MPP^+ 1.07 ± 0.04, p = 0.36 *vs.* baseline; 2-way ANOVA with Tukey multiple comparisons test; Fig. 5E). In contrast, a robust and highly significant increase was found in the dopaminergic neurons of α-Syn zebrafish under identical conditions (α-Syn post-MPP^+ 1.73 ± 0.09; $p < 10^{-15}$ *vs.* baseline, 2-way ANOVA with Tukey multiple comparisons test; Fig. 5E). Both the final roGFP2-Orp1 405/488 ratio ($p < 10^{-11}$, α-Syn *vs.* Ctrl, 2-way ANOVA with Tukey multiple comparisons test; Fig. 5E) and the fold increase from baseline within individual neurons (Ctrl 1.19 ± 0.04, α-Syn 1.86 ± 0.06; $p < 10^{-15}$, α-Syn *vs.* Ctrl, 2-tailed unpaired *t*-test; Fig. 5F) were significantly higher in α-Syn than Ctrl zebrafish. MPP^+ is selectively transported into dopaminergic neurons, so that no significant increase in roGFP2-Orp1 405/488 ratio was observed in non-dopaminergic neurons from either experimental group (baseline *vs.* post-MPP^+, Ctrl 1.15 ± 0.05 *vs.* 1.29 ± 0.13, p = 0.99; α-Syn 0.99 ± 0.03 *vs.* 1.21 ± 0.05, p = 0.99; 2-way ANOVA with Tukey multiple comparisons test; Fig. 5C, G). Together, these data show that cytoplasmic H_2O_2 flux induced by the mitochondrial complex I inhibitor MPP^+ in dopaminergic neurons was significantly augmented by α-Synuclein.

3.5. α-Synuclein-dependent H_2O_2 flux triggered by MPP^+ is mitigated by TEMPOL

We next employed 4-hydroxy-2,2,6,6-tetramethylpiperidin-1-oxyl (TEMPOL) to verify that the signal detected in these assays was attributable to generation of endogenous ROS. TEMPOL is a nitroxide with a broad range of actions in detoxifying ROS in living systems [70].

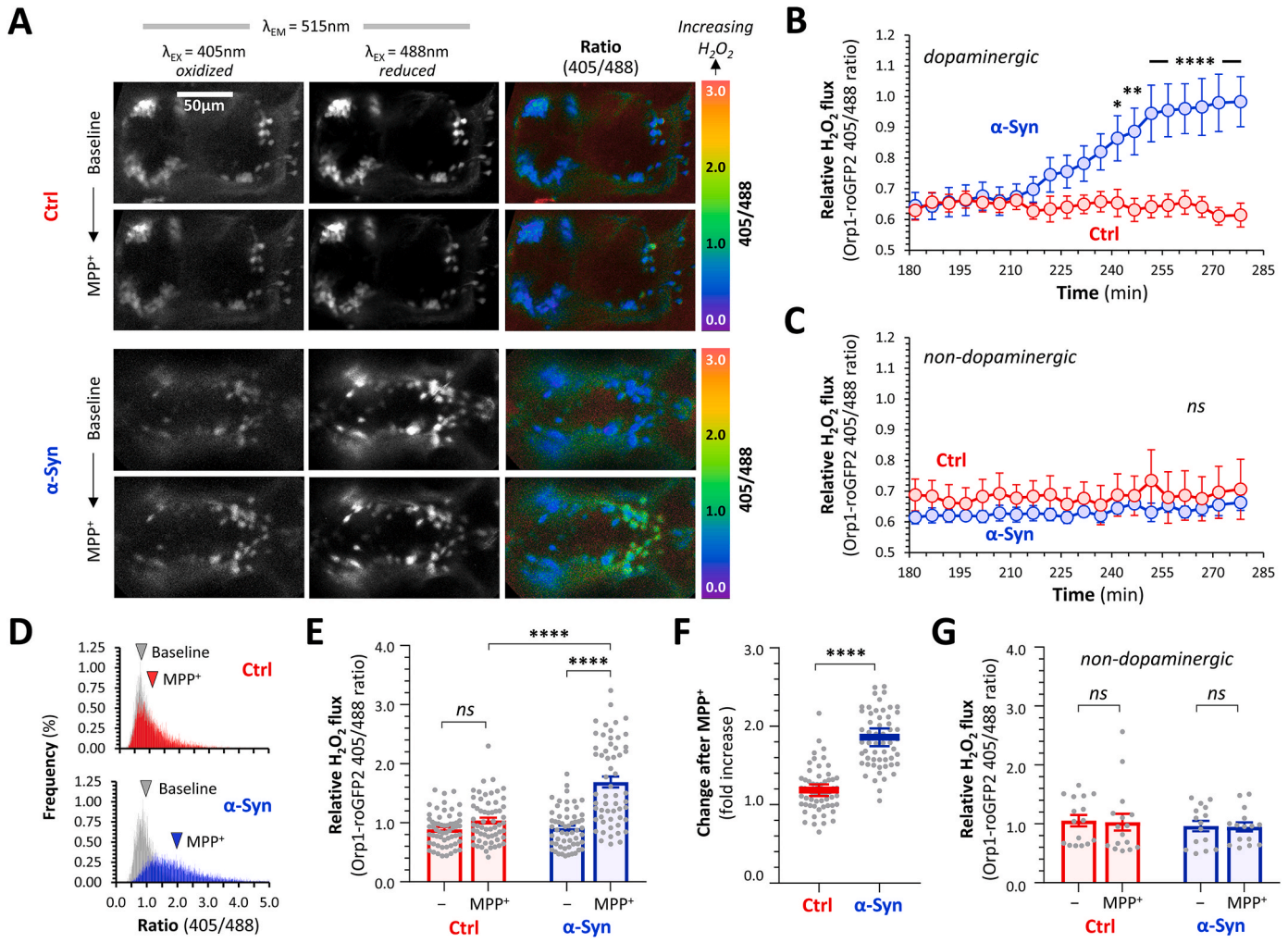

Fig. 5. α-Synuclein increases cytoplasmic peroxide flux in dopaminergic neurons exposed to MPP$^+$.

A: Intravital confocal microscopy was used to image the roGFP2-Orp1 biosensor dynamically in the ventral diencephalon of live Ctrl; roGFP2-Orp1 (upper six panels) and α-Syn; roGFP2-Orp1 (lower six panels) zebrafish, at baseline (upper row of each set) and following exposure to MPP$^+$ (lower row of each set; 3 mM final bath concentration). Emission at 515 nm following excitation at 405 nm and 488 nm respectively are shown in the first two columns and the ratiometric 405/488 images (color scale to right of images) in the third column of each set.

B, C: Using the unbiased 3D spot detection method, the roGFP2-Orp1 405/488 ratio was calculated for (C) dopaminergic DC4 – 6 neurons (n = 7 to 8) and (D) adjacent non-dopaminergic neurons (n = 6 to 8), in serial images acquired every ≈5 min over 5 h. After stable baseline data were collected, MPP$^+$ was added to the bath; the x-axis shows time after addition of MPP$^+$. Each data point shows mean ± SE; $p < 0.05$*, 0.01**, 0.0001**** Ctrl *vs.* α-Syn at same time point, 2-way repeated measures ANOVA with Šidák multiple comparisons test.

D: Ratiometric histograms showing the frequency distribution of the 405/488 ratio from every pixel within areas corresponding to DC4 – 6 dopaminergic neurons on 2D images at baseline (grey) and t = 280 min after addition of MPP$^+$ for Ctrl (red) and α-Syn (blue) zebrafish. The arrowheads show the mean of each distribution.

E: Scatterplot showing roGFP2-Orp1 405/488 ratio calculated using the 3D method, in DC4 – 6 dopaminergic neurons from Ctrl (blue) and α-Syn (red) zebrafish, at baseline and following exposure to MPP$^+$. Data points represent individual neurons (Ctrl n = 57; α-Syn n = 59 neurons, combined from 4 replicate zebrafish); bars show mean ± SE; $p < 0.001$**, 0.0001****, 2-way ANOVA with Tukey multiple comparison test.

F: Scatterplot showing fold increase in roGFP2-Orp1 405/488 ratio between baseline and post-MPP$^+$ exposure for each individual cell shown in panel E. Bars show mean ± SE; $p < 10^{-15}$ ****, 2-tailed unpaired *t*-test.

G: Scatterplot showing baseline and peak roGFP2-Orp1 405/488 ratio in non-dopaminergic diencephalic neurons following exposure to MPP$^+$, from the same zebrafish analyzed in panel E (n = 16 neurons per group). Data points, bars, and analysis identical to panel E.

Although frequently used as superoxide dismutase mimic, TEMPOL also metabolizes peroxide through a catalytic activity that mimics catalase, an indirect catalytic activity dependent on heme-containing proteins, and also stoichiometric effects. Critically, TEMPOL is not toxic to zebrafish and is cell-permeant allowing its use to mitigate ROS *in vivo*. α-Syn; roGPF2-Orp1 larvae were pre-treated with TEMPOL (3 mM in embryo water) or embryo water only for 16 h, then exposed acutely to MPP$^+$ while imaging the roGPF2-Orp1 biosensor to detect cytoplasmic peroxide (Fig. 6). Under these conditions, α-Syn zebrafish that had not been exposed to TEMPOL showed a progressive increase in the roGFP2-Orp1 405/488 ratio in their dopaminergic neurons following MPP$^+$ exposure (Fig. 6B), resulting in a highly significant increase relative to baseline during the recording (baseline *vs.* post-MPP$^+$: 0.80 ± 0.03 *vs.* 1.31 ± 0.05, $p < 10^{-12}$, 2-way ANOVA with Tukey's multiple comparisons test; Fig. 6C and D). In contrast, TEMPOL-exposed α-Syn zebrafish showed no increase in the roGFP2-Orp1 405/488 ratio under identical conditions (Fig. 6B) and no detectable change during the time course of the experiment (baseline *vs.* post-MPP$^+$: 0.70 ± 0.02 *vs.* 0.68 ± 0.02, p = 0.98, 2-way ANOVA with Tukey's multiple comparisons test; Fig. 6C and D). Compared with α-Syn zebrafish exposed to water only, the dopaminergic neurons of TEMPOL-exposed α-Syn zebrafish showed a significantly lower final Orp1 488/405 ratio ($p < 10^{-12}$, 2-way ANOVA

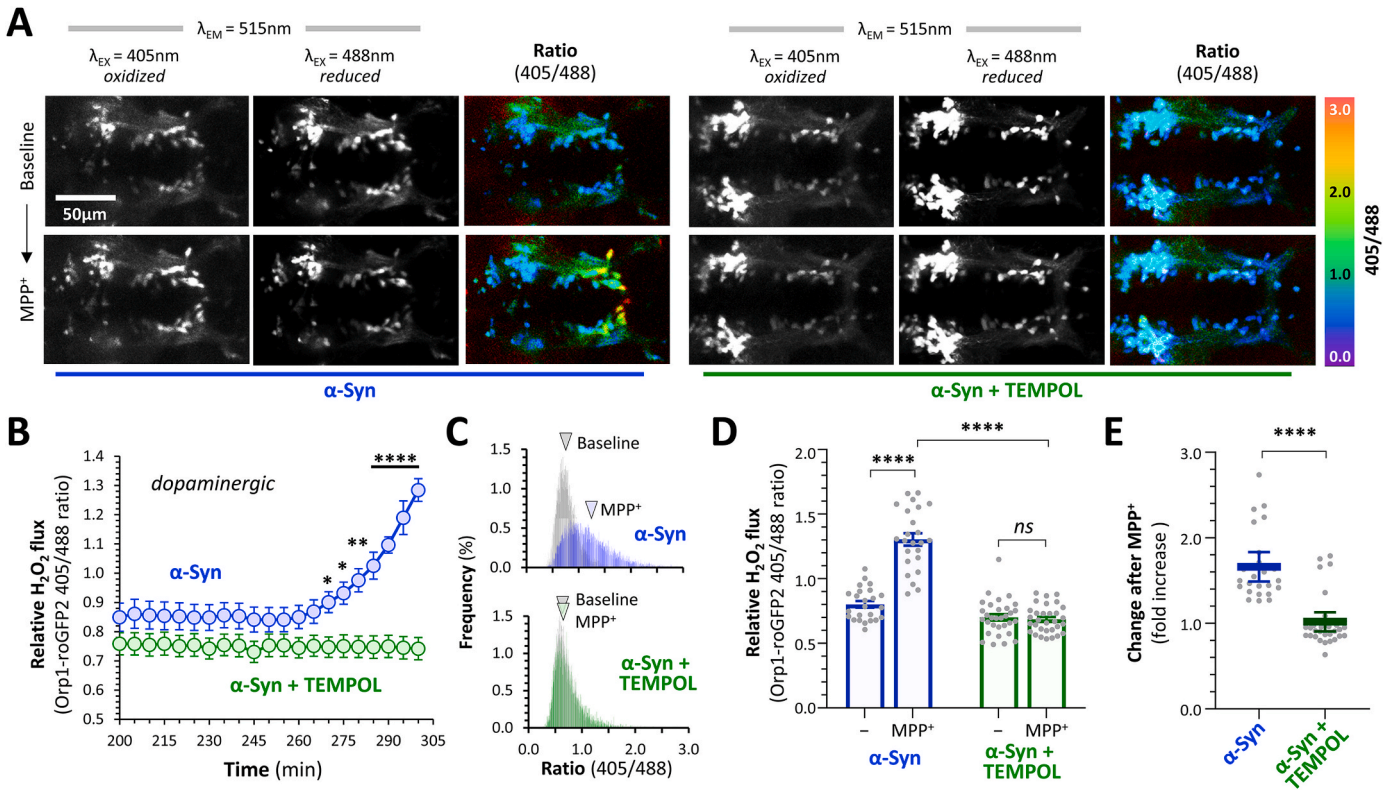

Fig. 6. TEMPOL prevents α-Synuclein-dependent cytoplasmic peroxide flux in dopaminergic neurons exposed to MPP$^+$.

A: Intravital confocal microscopy was used to image the roGFP2-Orp1 biosensor dynamically in the ventral diencephalon of live α-Syn; roGFP2-Orp1 zebrafish, following pretreatment with embryo water only (left six panels) or TEMPOL (3 mM in embryo water; right six panels), at baseline and following exposure to MPP$^+$ (3 mM final bath concentration). Emission at 515 nm following excitation at 405 nm and 488 nm respectively are shown in the first two columns and the ratiometric 405/488 images (color scale to right of images) in the third column of each image set.

B: Unbiased 3D spot detection was used to calculate the roGFP2-Orp1 405/488 ratio in dopaminergic DC4 – 6 neurons (n = 5 per group) in serial images acquired over 5 h after addition of MPP$^+$ to the bath (x axis shows time after addition of MPP$^+$). Mean ± SE roGFP2-Orp1 405/488 ratio is shown for neurons from α-Syn; Orp1-roGFP2 zebrafish that were pretreated with water only (blue) or TEMPOL (green). $P < 0.05$*, 0.01**, 0.0001**** water *vs.* TEMPOL at same time point, 2-way repeated measures ANOVA with Šidák multiple comparisons test.

C: Ratiometric histograms showing the frequency distribution of the roGFP2-Orp1 405/488 ratio from every pixel within areas corresponding to DC4 – 6 dopaminergic neurons on 2D images at baseline (grey) and t = 300 min after addition of MPP$^+$ for α-Syn zebrafish pretreated with water (blue) or TEMPOL (green). The arrowheads show the mean of each distribution.

D: Scatterplot showing roGFP2-Orp1 405/488 ratio calculated using the 3D method in DC4 – 6 dopaminergic neurons from α-Syn zebrafish pre-treated with water (blue; n = 24) or TEMPOL (green; n = 31 neurons), at baseline and following exposure to MPP$^+$. Data points represent individual neurons combined from 4 replicate zebrafish in each group; bars show mean ± SE; $p < 0.0001$****, 2-way ANOVA with Tukey multiple comparison test.

E: Scatterplot showing fold increase in roGFP2-Orp1 405/488 ratio between baseline and post-MPP$^+$ exposure for each individual cell shown in panel D. Bars show mean ± SE; $p < 0.0001$****, 2-tailed unpaired *t*-test.

with Tukey's multiple comparisons test; Fig. 6D) and fold induction over baseline for individual neurons (water 1.66 ± 0.08 *vs.* TEMPOL 1.02 ± 0.05, $p < 10^{-7}$, 2-tailed unpaired *t*-test; Fig. 6E). Since TEMPOL detoxifies a variety of reactive oxygen species, these data support the interpretation that the dramatic change in dynamic ratiometric Orp1-roGFP2 signal following MPP$^+$ exposure in dopaminergic neurons expressing α-Synuclein reflects detection of endogenous cytoplasmic peroxide flux.

3.6. α-Synuclein augments cytoplasmic H_2O_2 flux in DA neurons in vivo during prolonged exposure to MPP$^+$

To evaluate the effects of longer toxicant exposures and to exclude the possibility that serial imaging (with repeated laser excitation of the roGFP2 fluorophore) contributed to the observed changes in roGFP2-Orp1 oxidation, we next determined integrated relative cytoplasmic peroxide flux at a single time point following prolonged exposure to MPP$^+$, relative to control zebrafish maintained in embryo buffer without MPP$^+$ (vehicle control). We previously showed that exposure to MPP$^+$ at low concentrations for 16 h causes significant changes in the mitochondrial dynamics of zebrafish dopaminergic neurons without provoking cell death, providing a convenient model to examine mechanisms of mitochondrial pathogenesis in the degeneration of dopaminergic neurons [18].

We first confirmed that α-Syn zebrafish did not show evidence of dopaminergic neuronal loss that would preclude imaging studies following prolonged low-level MPP$^+$ exposure (supplemental figure 5). Next, we imaged the roGFP2-Orp1 biosensor in multiple α-Syn and Ctrl zebrafish following exposure to MPP$^+$ or vehicle. Representative 2D pixel-wise analyses (Fig. 7A) showed a rightwards shift in the roGFP2-Orp1 405/488 ratiometric distribution following MPP$^+$ exposure that was more prominent in dopaminergic neurons expressing α-Synuclein. 3D single-cell analysis of zebrafish pooled from multiple experiments (n = 180 – 470 neurons/group) showed no difference in the roGFP2-Orp1 405/488 ratio between dopaminergic neurons of α-Syn and Ctrl zebrafish exposed to vehicle only (Ctrl 0.84 ± 0.02 *vs.* α-Syn 0.86 ± 0.02, $p = 0.98$, 1-way ANOVA with Tukey multiple comparisons test; Fig. 7B). Relative to vehicle-exposed zebrafish, both Ctrl and α-Syn zebrafish showed evidence of enhanced cytoplasmic peroxide flux following prolonged low-level MPP$^+$ exposure (Ctrl 1.06 ± 0.02, $p < 10^{-5}$ *vs.*

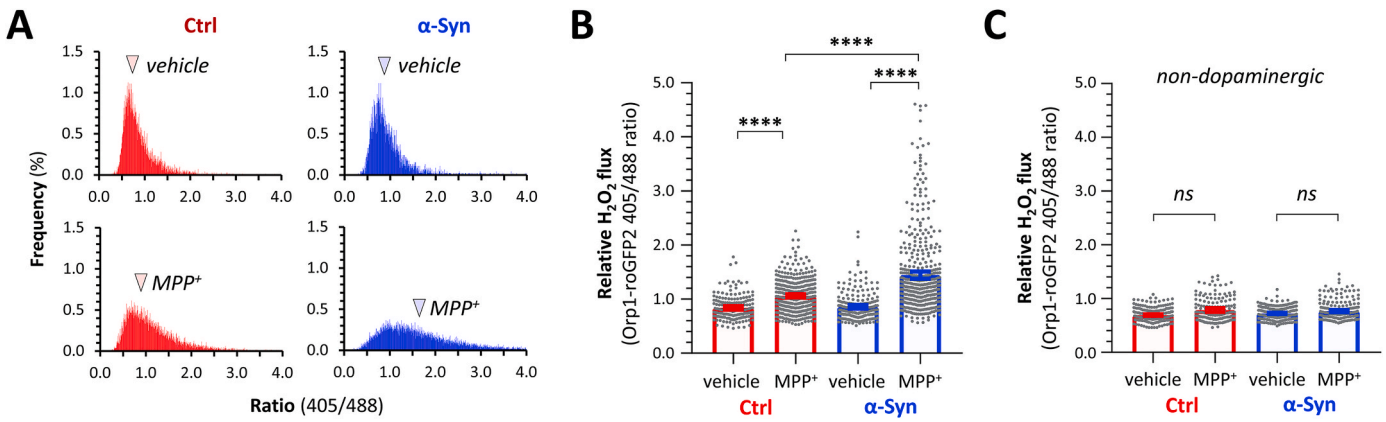

Fig. 7. α-Synuclein enhances cytoplasmic peroxide flux in dopaminergic neurons during prolonged MPP^+ exposure.
Ctrl; roGFP2-Orp1 (red) and α-Syn; roGFP2-Orp1 (blue) zebrafish were exposed to vehicle (embryo water only) or MPP^+ (0.5 mM bath concentration) for 16 h and then the ro-GFP2-Orp1 biosensor imaged in live intact larvae at a single time point. Emission at 515 nm following sequential excitation at 405 nm and 488 nm was recorded as shown in Figs. 4–6.

A: Histograms showing the frequency distribution of the ro-GFP2-Orp1 405/488 ratio from every pixel within areas corresponding to DC4 – 6 dopaminergic neurons within 2D images from Ctrl (red, left column) and α-Syn (right, blue) zebrafish exposed to vehicle (upper row) or MPP^+ (lower row). The arrowheads show the mean of each distribution.

B, C: Scatterplots showing roGFP2-Orp1 405/488 ratio calculated from 3D image analysis, in (B) DC4 – 6 dopaminergic neurons and (C) adjacent non-dopaminergic neurons, from Ctrl (red) and α-Syn (blue) zebrafish exposed to vehicle or MPP^+ for 16 h. Data points represent individual neurons (dopaminergic: Ctrl vehicle n = 181; Ctrl MPP^+ n = 379; α-Syn vehicle n = 210; α-Syn MPP^+ n = 470; non-dopaminergic: Ctrl vehicle n = 208; Ctrl MPP^+ n = 156; α-Syn vehicle n = 254; α-Syn MPP^+ n = 225 neurons, combined from 10 to 13 replicate zebrafish in each group); bars show mean ± SE; $p < 0.0001$****, 1-way ANOVA with Tukey multiple comparisons test.

vehicle; α-Syn 1.44 ± 0.03, $p < 10^{-15}$ *vs.* vehicle; 1-way ANOVA with Tukey multiple comparisons test; Fig. 7B). Similar to our observations in acute exposure experiments, however, the roGFP2-Orp1 405/488 ratio following MPP^+ exposure was significantly higher in α-Syn than in Ctrl zebrafish ($p < 10^{-15}$ Ctrl vs. α-Syn; 1-way ANOVA with Tukey multiple comparisons test; Fig. 7B). There were no changes in roGFP2-Orp1 405/488 ratio in non-dopaminergic neurons attributable to α-Synuclein expression or MPP^+ exposure (Fig. 7C). Together, these data suggest that the rate of cytoplasmic peroxide flux in dopaminergic neurons in the presence of prolonged MPP^+ exposure was enhanced in cells expressing α-Synuclein. These data also exclude the possibility that progressive changes in roGFP2-Orp1 oxidation in our dynamic imaging experiments were caused by repeated exposure of the fluorophore to the excitation laser.

3.7. *α-Synuclein increases cytoplasmic H_2O_2 flux in dopaminergic neurons exposed to rotenone*

In order to verify that data from zebrafish exposed to MPP^+ were relevant to understanding our observations in the rat model, we carried out additional studies in α-Syn and Ctrl zebrafish exposed to rotenone. Rotenone, a commonly-used piscicide, is highly toxic to zebrafish larvae through non-neurological mechanisms and consequently has not been used successfully to model parkinsonism in zebrafish (reviewed in Ref. [2]). In order to circumvent this problem, we employed low concentrations of rotenone that did not provoke overt systemic toxicity or compromise viability. α-Syn and Ctrl zebrafish were imaged in tandem at baseline and then rotenone (final concentration 80 nM) was added to the bath. Serial time-lapse imaging showed that the roGFP2-Orp1 405/488 ratio remained stable within dopaminergic neurons of both α-Syn and Ctrl zebrafish for the first 4 h of exposure (Fig. 8A). Between 5 and 8 h after the addition of rotenone, a gradual increase in cytoplasmic H_2O_2 flux was observed in both α-Syn and Ctrl zebrafish. Interestingly, rotenone also increased roGFP2-Orp1 oxidation in non-dopaminergic cells, compatible with its ubiquitous cellular permeability (Fig. 8C). The rate of increase of the roGFP2-Orp1 405/488 ratio accelerated in α-Syn zebrafish after 8 h, so the curves for α-Syn and Ctrl zebrafish diverged. By the end of the recording, there was a significant difference in integrated cytoplasmic peroxide flux between the dopaminergic neurons of Ctrl and α-Syn zebrafish (baseline: Ctrl 0.48 ± 0.03, α-Syn 0.54 ± 0.05, p = 0.58; post-rotenone: Ctrl 0.91 ± 0.05, α-Syn 1.10 ± 0.06, p = 0.023; 2-way repeated measures ANOVA with Šidák multiple comparisons test; Fig. 8A, B). A similar trend was apparent in non-dopaminergic neurons, although the difference between Ctrl and α-Syn was not statistically significant (Fig. 8C, D).

Given the significant technical challenges and low experimental throughput inherent in stable intravital imaging for periods of up to 12 h, we instead carried out single time point imaging in α-Syn and Ctrl zebrafish after exposure to vehicle or 80 nM rotenone for 16 h. Pixel-by-pixel analysis demonstrated that, compared with vehicle, rotenone exposure caused a large shift in the roGFP2-Orp1 405/488 ratiometric distribution towards oxidation in the dopaminergic neurons of α-Syn zebrafish, whereas a smaller change was apparent in Ctrl zebrafish (Fig. 8E). 3D analysis of individual cells from replicate experiments showed that rotenone provoked a significant increase in the roGFP2-Orp1 ratio in dopaminergic neurons of both Ctrl (vehicle 0.30 ± 0.01, rotenone 0.56 ± 0.02, $p < 10^{-5}$, 1-way ANOVA with Tukey multiple comparison test; Fig. 8F) and α-Syn (vehicle 0.44 ± 0.01, rotenone 0.87 ± 0.02, $p < 10^{-9}$, 1-way ANOVA with Tukey multiple comparison test; Fig. 8F) zebrafish. The rotenone-induced increase was more prominent in dopaminergic neurons from α-Syn than Ctrl zebrafish (post-rotenone 405/488 ratio Ctrl vs. α-Syn, $p < 10^{-9}$, 1-way ANOVA with Tukey multiple comparison test; Fig. 8F). Similar, but less dramatic, changes were also seen in non-dopaminergic neurons (Fig. 8G). Together, these data show that α-Synuclein increases rotenone-induced cytoplasmic peroxide flux in CNS neurons *in vivo* and the effect is more prominent in dopaminergic than non-dopaminergic neurons.

To summarize, the experiments in Figs. 5–8 illustrate both dynamic time-lapse and single time-point intravital ratiometric imaging studies, following acute or prolonged exposure to two different mitochondrial complex I inhibitors implicated in parkinsonism. Overall, the data show unequivocally that α-Synuclein amplifies cytoplasmic peroxide flux in dopaminergic neurons *in vivo*, following inhibition of mitochondrial complex I by chemical toxicants.

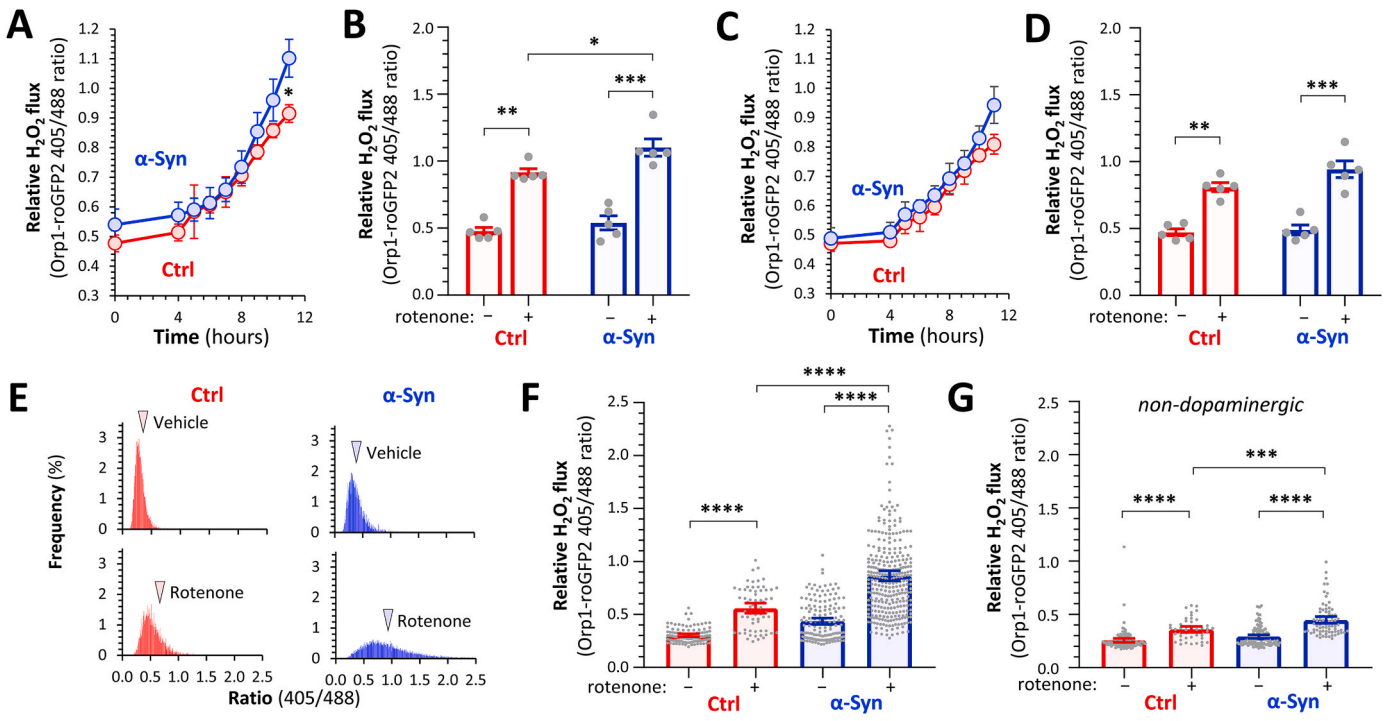

Fig. 8. α-Synuclein enhances cytoplasmic peroxide flux in dopaminergic neurons following rotenone exposure.

A – D: The roGFP2-Orp1 biosensor was imaged by intravital confocal microscopy in the ventral diencephalon of live Ctrl; roGFP2-Orp1 (red) and α-Syn; roGFP2-Orp1 (blue) zebrafish, at baseline and serially for 11 h after addition of rotenone to the bath (80 nM final concentration). 3D ratiometric analyses are shown for (A, B) DC4 – 6 dopaminergic neurons and (C, D) adjacent non-dopaminergic neurons (n = 5 neurons in each group). (A) and (C) show mean ± SE roGFP2-Orp1 405/488 ratio at each time point; $p < 0.05$* α-Syn *vs.* Ctrl at same time point, 2-way repeated measures ANOVA with Šidák multiple comparisons test. (B) and (D) show baseline and final roGFP2-Orp1 405/488 ratio; data points show individual neurons, bars show mean ± SE; $p < 0.05$*, 0.01**, 0.001***, 2-way ANOVA with Tukey multiple comparisons test.

E – G: Ctrl; roGFP2-Orp1 (red) and α-Syn; roGFP2-Orp1 (blue) zebrafish were exposed to vehicle or rotenone (80 nM bath concentration) for 16 h and then the roGFP2-Orp1 imaged in live intact larvae by intravital confocal microscopy at a single time point. (E) Frequency distribution histograms from pixel-by-pixel 2D ratiometric analyses of DC4 – 6 dopaminergic neurons in vehicle-exposed (upper row) compared with rotenone-exposed (lower row) zebrafish. Arrowheads show the mean of each distribution. (F, G) 3D analysis of roGFP2-Orp1 405/488 ratios for (F) dopaminergic and (G) non-dopaminergic neurons. Data points show individual neurons (dopaminergic: Ctrl vehicle n = 107; Ctrl rotenone n = 66; α-Syn vehicle n = 154; α-Syn rotenone n = 304; non-dopaminergic: Ctrl vehicle n = 111; Ctrl rotenone n = 46; α-Syn vehicle n = 117; α-Syn rotenone n = 80 neurons, combined from 7 to 11 replicate zebrafish in each group); bars show mean ± SE; $p < 0.05$*, 0.0001****, 1-way ANOVA with Tukey multiple comparisons test.

3.8. *Transgenic zebrafish expressing a biosensor for glutathione oxidation*

We next evaluated the role of α-Synuclein in cellular oxidative stress, by generating transgenic zebrafish expressing a dynamic ratiometric reporter of glutathione oxidation. Grx1-roGFP2 is a fusion protein in which glutaredoxin-1 is fused to roGFP2, so that formation of a disulfide bond within the roGFP2 fluorophore is favored under conditions in which cellular glutathione is oxidized [22]. The reaction is reversible, so the Grx1-roGFP2 405/488 ratio reports the redox potential of the glutathione redox couple, which is dependent on both the ratio of oxidized (GS-SG) to reduced (GSH) glutathione and the cellular GSH concentration. The biosensor can report nanomolar changes in cellular GS-SG rapidly in response to redox perturbations [22,43].

Tg(*UAS:Grx1-roGFP2*) zebrafish were generated on the transparent Casper (*roy*$^{-/-}$*; nacre*$^{-/-}$) background [69] then crossed with Tg(*otpb:gal4*); Tg(*UAS:mCherry*) and Tg(*otpb:gal4*); Tg(*UAS:hsa.SNCA--p2A-nls-mCherry*) zebrafish to generate Ctrl; Grx1-roGFP2 and α-Syn; Grx1-roGFP2 zebrafish, similar to the construction of roGFP2-Orp1 lines described above. Immunofluorescence analysis of fixed tissue (Fig. 9A) confirmed Grx1-roGFP2 and mCherry co-expression in the ventral diencephalon of both α-Syn and Ctrl zebrafish, within both TH-expressing DC4 – 6 dopaminergic neurons and an adjacent group of non-dopaminergic cells.

Live imaging was carried out using identical methods to those employed in imaging the roGFP2-Orp1 biosensor described above. Addition of H_2O_2 to the bath provoked an increase in the roGFP2 signal after excitation at 405 nm, and a decrease in the signal after excitation at 488 nm, resulting in a strong increase in the 405/488 ratio (shown in the colormap images of Fig. 9B). The signals were quantified using the same methods as deployed for the roGFP2-Orp1 biosensor. Analysis of cells by unbiased 3D spot detection illustrated dynamic changes in the raw signal from each image channel and a robust increase in the Grx1-roGFP2 405/488 ratio after H_2O_2 application (Fig. 9C, E). These findings were reflected in a rightwards shift in the ratiometric pixel-wise histogram from 2D image analyses (Fig. 9D). After H_2O_2 exposure sufficient to cause significant Grx1-roGFP2 oxidation, medium containing H_2O_2 was replaced with fresh medium containing TEMPOL. This resulted in a rapid restoration of the 405nm/488 nm ratio to baseline values (Fig. 9C, E). Together these data show that the Grx1-roGFP2 reporter functions as a reversible biosensor of oxidative stress in the zebrafish CNS *in vivo*.

3.9. *α-Synuclein potentiates oxidative stress following application of exogenous ROS in vivo*

Finally, we asked whether oxidative stress in dopaminergic neurons at baseline and following an oxidative challenge was modulated by α-Synuclein. For these experiments, instead of imaging responses to the production of endogenous ROS following exposure to mitochondrial inhibitors (which differs between α-Syn and Ctrl zebrafish), we

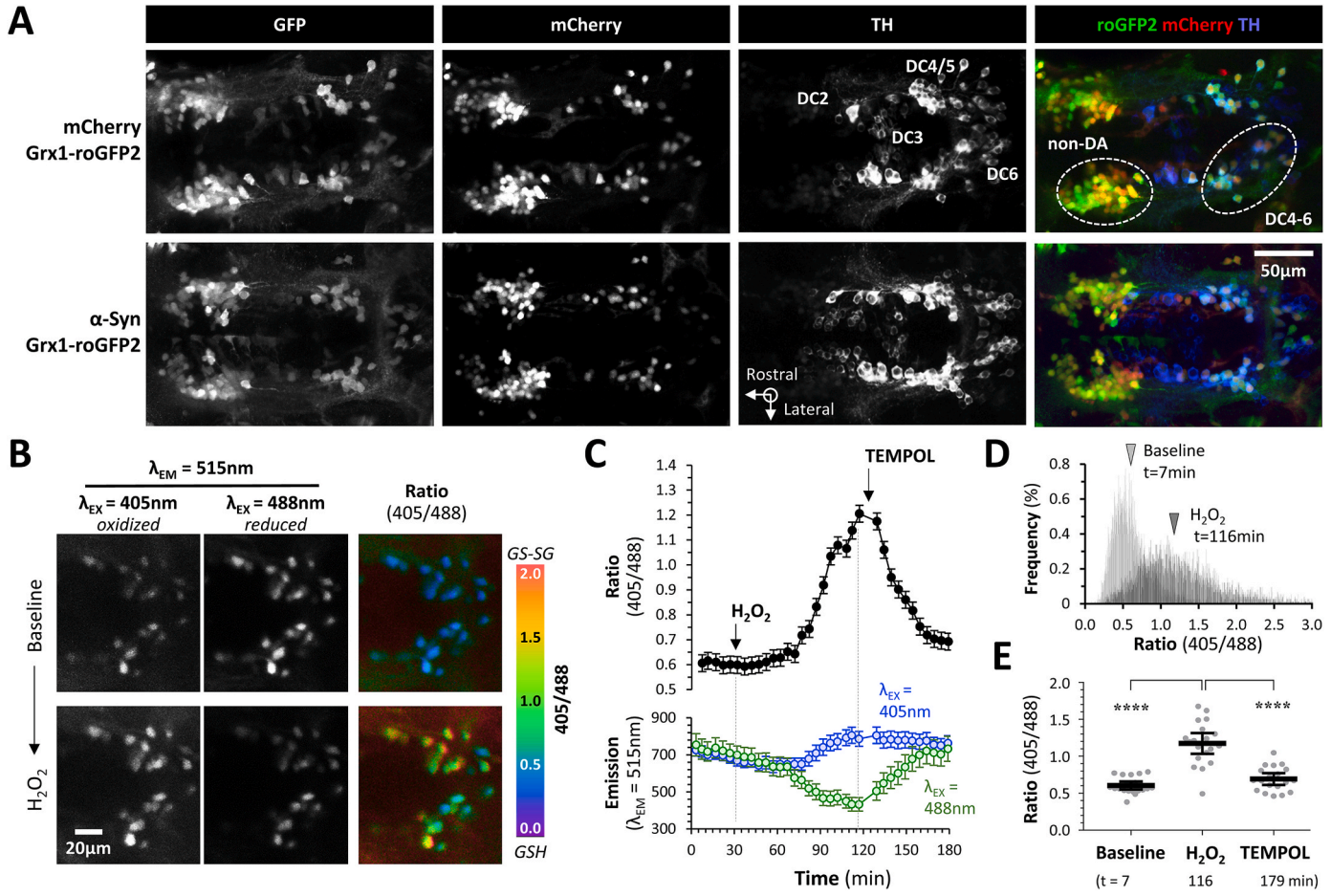

Fig. 9. Transgenic zebrafish expressing human α-Synuclein and a ratiometric biosensor of glutathione oxidation in dopaminergic neurons *in vivo*.
A: Confocal z-plane projections of fixed, whole mount Ctrl; Grx1-roGFP2 (upper row) and α-Syn; Grx1-roGFP2 (lower row) zebrafish labeled with antibodies to GFP, mCherry and tyrosine hydroxylase. The overlaid images are shown in the right column (GFP, green; mCherry, red; TH, blue). Groups of TH-expressing diencephalic dopaminergic neurons that also express the *otpb* enhancer element used in the driver line are numbered in the Ctrl TH image. The Ctrl overlay image indicates the locations of the DC 4–6 dopaminergic neurons imaged in live zebrafish in Fig. 10 and a more rostral group of non-dopaminergic neurons (non-DA) that also expresses the *otpb* enhancer and was imaged for comparison.
B: Intravital confocal microscopy was used to image the Grx1-roGFP2 biosensor in the ventral diencephalon of an α-Syn; Grx1-roGFP2 zebrafish. Emission was captured at 515 nm following serial excitation at 405 nm (left column) and 488 nm (center column). The ratiometric image (right column; color scale shown to the right), calculated by dividing each image plane of the 405 nm dataset by the corresponding 488 nm image plane, shows the relative glutathione redox potential. The images show the dopaminergic DC4 – 6 neuronal groups; the top row shows baseline steady-state images and the bottom row shows images of the same zebrafish after application of 3 mM H_2O_2 to the bath.
C: Unbiased 3D spot detection was used to quantify emission at 515 nm within DC4 – 6 dopaminergic neurons, following sequential excitation at 405 nm or 488 nm (bottom graph) and to calculate the 405/488 ratio (top graph) in serial images acquired every 4 min for 1 h. Each datapoint shows mean ± SE (n = 19 neurons). After stable baseline data were collected, H_2O_2 was added to the bath at t = 30 min and then H_2O_2 was removed and TEMPOL added to the bath at 120 min (arrows).
D: Ratiometric histograms showing the frequency distribution of the Grx1-roGFP2 405/488 ratio from every pixel within areas corresponding to DC4 – 6 dopaminergic neurons in 2D images, at baseline (top panel) and after addition of H_2O_2 to the bath (bottom panel). The arrowheads show the mean of each distribution.
E: Scatterplots showing baseline, peak and final Grx1-roGFP2 405/488 ratio in DC4 – 6 dopaminergic neurons following sequential exposure to H_2O_2 and TEMPOL. Data points represent individual neurons combined from 4 separate zebrafish; bars show mean ± SE; $p < 0.0001$****, 1-way ANOVA with Tukey multiple comparison test.

evaluated the change in cellular glutathione redox potential in response to application of an exogenous ROS challenge. α-Syn; Grx1-roGFP2 and Ctrl; Grx1-roGFP2 zebrafish were embedded adjacent to one another in a glass-bottom dish and dynamic intravital imaging carried out in tandem following addition of H_2O_2 to the bath, ensuring that experimental conditions were identical between the two experimental groups. Both dopaminergic and non-dopaminergic neurons showed changes in the individual channels and in the Grx1-roGFP2 405/488 ratio in response to exogenous H_2O_2 (Fig. 10A). However, expression of α-Synuclein increased the amount by which the ratiometric Grx1-roGFP2 signal changed between baseline and peak. This was apparent in both the ratiometric images and ratiometric histograms derived from 2D image analysis (Fig. 10A and B). 3D analysis to quantify the Grx1-roGFP2 405/488 ratio in individual dopaminergic neurons showed no significant baseline difference in Grx1-roGFP2 405/488 ratio between Ctrl and α-Syn zebrafish (Ctrl 0.82 ± 0.06 *vs.* α-Syn 1.13 ± 0.08, p = 0.36; 2-way ANOVA with Tukey multiple comparison test; Fig. 10C). Exposure to H_2O_2 was associated with a trend towards a higher Grx1-roGFP2 405/488 ratio in the dopaminergic neurons of Ctrl zebrafish (1.09 ± 0.07, $p = 0.56$ *vs.* baseline; 2-way ANOVA with Tukey multiple comparison test; Fig. 10C) and a dramatic and highly-significant increase in the dopaminergic neurons of α-Syn zebrafish (3.07 ± 0.18, $p < 10^{-12}$ *vs.* baseline; 2-way ANOVA with Tukey multiple comparison test; Fig. 10C). The post-H_2O_2 Grx1-roGFP2 405/488 ratio in dopaminergic neurons expressing α-Synuclein greatly exceeded that of Ctrl neurons expressing only mCherry ($p < 10^{-12}$ Ctrl vs. α-Syn; 2-way ANOVA with Tukey multiple

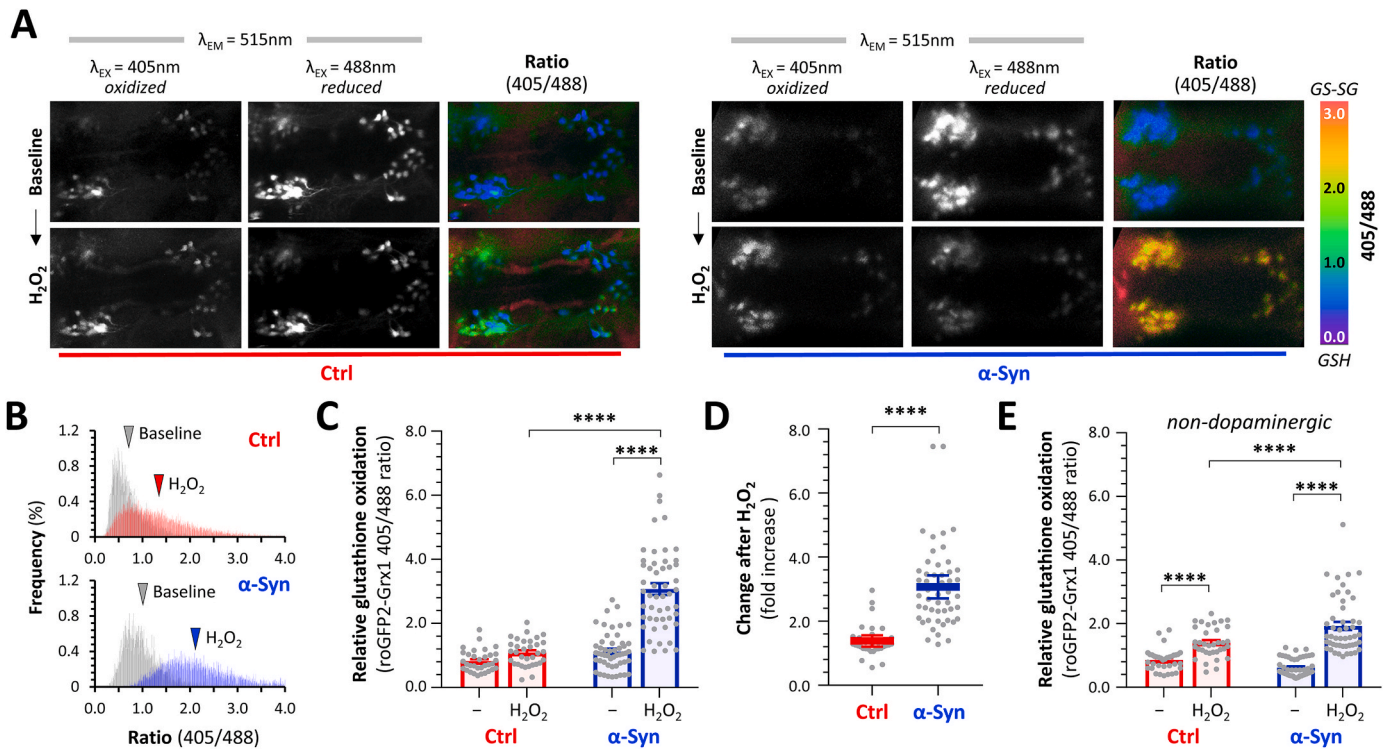

Fig. 10. α-Synuclein enhances H_2O_2-induced glutathione oxidation in dopaminergic neurons *in vivo*.

A: Intravital confocal microscopy was used to image the Grx1-roGFP2 biosensor in the ventral diencephalon of live Ctrl; Grx1-roGFP2 (left six images) and α-Syn; Grx1-roGFP2 (right six images) zebrafish. Emission was captured at 515 nm following serial excitation at 405 nm (left column of each set) and 488 nm (center column of each set). The ratiometric image (right column of each set; color scale shown to the right), calculated by dividing each image plane of the 405 nm dataset by the corresponding 488 nm image plane, shows relative glutathione redox potential. The top row of images shows baseline steady-state images; the bottom row shows images of the same zebrafish after application of 3 mM H_2O_2 to the bath.

B: Ratiometric histograms showing the frequency distribution of the Grx1-roGFP2 405/488 ratio from every pixel within areas corresponding to DC4 – 6 dopaminergic neurons in 2D images, in Ctrl (top panel) and α-Syn zebrafish (bottom panel), at baseline (gray) and after H_2O_2 exposure (colored). The arrowheads show the mean of each distribution.

C: Scatterplot showing Grx1-roGFP2 405/488 ratio calculated using the 3D method, in DC4 – 6 dopaminergic neurons, at baseline and following exposure to H_2O_2. Data points represent individual neurons (Ctrl n = 33; α-Syn n = 51 neurons, combined from 4 replicate zebrafish in each group); bars show mean ± SE; $p < 0.01$**, 0.0001****, 2-way ANOVA with Tukey multiple comparison test.

D: Scatterplot showing fold increase in Grx1-roGFP2 405/488 ratio between baseline and post-H_2O_2 peak for each individual cell from panel C. Bars show mean ± SE; $p < 10^{-10}$ ****, 2-tailed unpaired *t*-test.

E: Scatterplot showing Grx1-roGFP2 405/488 ratio calculated using the 3D method, in non-dopaminergic neurons following exposure to H_2O_2. Data points represent individual neurons (Ctrl n = 35; α-Syn n = 49 neurons, combined from 4 replicate zebrafish in each group); bars show mean ± SE; $p < 0.01$**, 0.0001****, 2-way ANOVA with Tukey multiple comparisons test.

comparison test; Fig. 10C) as did the fold increase in individual neurons between baseline and peak (Ctrl 1.38 ± 0.09, α-Syn 3.05 ± 0.19; $p < 10^{-11}$; 2-tailed unpaired *t*-test; Fig. 10D). A similar, but more modest, difference was apparent in non-dopaminergic neurons (Fig. 10E).

Together, these data show that dopaminergic neurons of α-Syn zebrafish demonstrated significantly greater change in glutathione redox potential than Ctrl neurons following an identical H_2O_2 exposure. These findings suggest that α-Synuclein impairs the capacity of dopaminergic neurons to compensate for a redox perturbation, in addition to augmenting the peroxide load resulting from exposure to mitochondrial inhibitors.

4. Discussion

Our data show that dopaminergic neuronal dysfunction following exposure to rotenone is associated with α-Synuclein-dependent thiol oxidation in a rat model of PD. The dependence of these oxidative changes on α-Synuclein is likely attributable to two related mechanisms, revealed *in vivo* using novel zebrafish models. First, α-Synuclein amplified cytoplasmic peroxide flux in dopaminergic neurons following exposure to mitochondrial complex I inhibitors. Second, α-Synuclein enhanced perturbation of the glutathione redox potential in dopaminergic neurons following challenge with exogenous peroxide. These findings are important because they suggest that α-Synuclein plays a critical role in determining the cellular consequences of mitochondrial dysfunction in PD pathogenesis, and indicate that neuronal dysfunction secondary to oxidative stress precedes neurodegeneration, potentially providing a window of opportunity to prevent disease progression.

To the best of our knowledge, this is the first time that peroxide fluxes and changes in glutathione redox potential have been demonstrated dynamically at cellular resolution in the intact vertebrate CNS *in vivo*. Recording the modest signals generated by genetically-encoded redox biosensors in deep-lying neuronal groups *in vivo* is technically non-trivial, particularly since the short-wavelength light used to excite roGFP2 is poorly tissue-penetrant. However, by optimizing zebrafish genetics to increase signal and deploying imaging technologies to enhance signal detection and decrease noise, we were able to quantify roGFP2 ratiometric signals robustly by intravital microscopy. The new transgenic lines and experimental methods we report provide a powerful toolbox for understanding the dynamic role of ROS signaling in the living brain. Since the transgenic lines were made using Gal4/UAS genetics, the redox biosensors can be expressed in any other tissue of

interest by crossing the responder lines with an appropriate Gal4 driver, expanding the utility of these lines for future studies in other organ systems. Coupled with other new transgenic lines that allow targeted induction of chemoptogenetic damage to mitochondria in specific cells of a live zebrafish [73], these resources will be valuable for future studies to define sources, targets, and consequences of ROS signals *in vivo*.

The Orp1-roGFP2 fusion protein serves as a stoichiometric peroxide biosensor, through efficient dithiol-disulfide exchange between Orp1 and cysteine residues within the roGFP2 fluorophore [23,43]. The oxidation of Orp1-roGFP2 by peroxide is chemically irreversible, although Orp1 can be recycled enzymatically by Trx1 *in vivo* [43]. Our experience suggests that, at least in CNS neurons, the regeneration of reduced Orp1-roGFP2 is relatively inefficient: we only observed reversal of the Orp1-roGFP2 405/488 ratio many hours after withdrawal of an oxidative stimulus (during which time it is likely that new protein was synthesized in the cell, in addition to reduction of disulfide bonds), although the ratiometric signal reverted to baseline rapidly in the presence of a strong reducing agent such as DTT. Consequently, under the conditions used in these experiments, Orp1-roGFP2 serves as a biosensor of integrated peroxide flux. In this context, our data unequivocally indicate that cytoplasmic peroxide flux is amplified in dopaminergic neurons *in vivo* in the presence of α-Synuclein. The effect was robust, observed after exposure to two different complex I inhibitors implicated in PD, and detected in both acute exposure/dynamic imaging and prolonged exposure/static imaging paradigms. Several possible molecular mechanisms could explain these observations.

One interpretation is that mitochondrial ROS formation was amplified by α-Synuclein. O_2 can acquire electrons to form superoxide or peroxide at any of eleven identified points in the electron transport chain (ETC) upstream of complex IV [7]. This 'electron leak' is regulated by substrate availability and ATP demand, and has known physiological functions: for example, HIFα signaling depends on superoxide formation at complex III in the presence of tissue hypoxia [10]. Rotenone and MPP^+ both bind to complex I near to the ubiquinone-binding site [53], preventing transfer of electrons to ubiquinone and consequently increasing the formation of superoxide at the flavin mononucleotide-containing NADH binding site in the mitochondrial matrix [7]. Disruption of electron transport at complex I also enhances ROS production at additional electron leak sites within the 2-oxoacid--dehydrogenases that transfer electrons from TCA cycle substrates to NADH [52]. It is possible that α-Synuclein interacts directly or indirectly with proteins adjacent to these sites to promote electron transfer to O_2 in the presence of ETC inhibitors. There is evidence that α-Synuclein can associate with or enter mitochondria [13,16,40,57] and inhibit complex I activity [16,42], although the possibility that α-Synuclein influences electron leak directly at, or upstream of, complex I has not been addressed. An alternative consideration relates to mitochondrial protein import. We showed previously that oligomeric and dopamine-modified α-Synuclein inhibit mitochondrial protein import by binding to the TOM20 component of the translocase complex [17]. Complex I contains 38 nuclear-encoded proteins that are imported from the cytoplasm to the mitochondrial matrix, so that correct assembly of the complex is vulnerable to factors that inhibit protein import. Mitochondrial localization of the NDUFS3 subunit of complex I was decreased in PD tissue and in cultured cells in the presence of oligomeric α-Synuclein, and this was associated with impaired cellular respiration and evidence of oxidative stress [17]. It will be of interest to determine whether oligomeric or DA-modified forms of α-Synuclein are present in the zebrafish model, and to investigate the expression and localization of complex I components in the dopaminergic neurons of α-Synuclein-expressing zebrafish.

Peroxide production triggered elsewhere in the cell by the initial rotenone/MPP^+-provoked mitochondrial ROS burst might also be influenced by α-Synuclein. NADPH oxidases are the principal non-mitochondrial source of ROS. NADPH oxidase activity was induced by ROS in cultured tumor cells [37,39]; furthermore, NOX1 expression was suppressed by loss of mtDNA (and therefore ETC function) and upregulated by rotenone, correlating with mitochondrial superoxide production [15]. Neurons express NOX1 and NOX4, and both isoenzymes were upregulated and translocated to the nucleus in PD substantia nigra [12,74]. NOX1 also showed nuclear translocation in cultured N27 cells and mouse substantia nigra exposed to 6-hydroxydopamine, and contributed to neurotoxicity and α-Synuclein aggregation in rodent 6-OHDA and paraquat models [12,14]. In addition, microglial NOX2 in the substantia nigra was upregulated in PD tissue, and in mice exposed to MPTP. Both loss of dopaminergic neurons and oxidative damage to proteins in this model were partially mitigated on a NOX2-null genetic background [72]. α-Synuclein is known to upregulate NOX2 in cultured microglial cells [29,31] and a peptide fragment of α-Synuclein has been reported to bind to microglial NOX2 directly [67]. These data suggest that both neuronal and microglial NADPH oxidases may contribute to ROS fluxes in dopaminergic neurons triggered by mitochondrial inhibitors and provide some intriguing possibilities for how α-Synuclein might modulate non-mitochondrial sources of peroxide. However, whether α-Synuclein directly influences localization, assembly, activity, or expression of NADPH oxidases, or modulates mitochondrial-NOX signaling, is currently uncertain. These are important questions to be addressed in future studies, which will be facilitated by the extensive phylogenetic conservation and CNS expression of NOX isoenzymes in the zebrafish model [68].

Enhanced peroxide flux might also be detected in the presence of normal rates of production if elimination is decreased. The majority of mitochondrial superoxide and peroxide is detoxified before egress to the cytoplasm, through enzymatic degradation (by superoxide dismutase and catalase) or through chemical reaction with glutathione. The roGFP2-Grx1 biosensor we employed reports the redox potential of the GSH/GSSG couple in the cytoplasm, which is influenced by both the oxidation status of glutathione and its cellular abundance [43]. α-Synuclein did not alone provoke detectable peroxide flux or change the cytoplasmic glutathione redox potential in the zebrafish model; however, although the roGFP2-Orp1 biosensor detected exogenous peroxide similarly in α-Syn and Ctrl zebrafish, an identical challenge provoked a significantly larger perturbation in glutathione oxidation status in α-Syn zebrafish, suggesting that glutathione homeostasis in dopaminergic neurons was dysregulated by α-Synuclein. Relative to other parts of the CNS, glutathione is less abundant in the substantia nigra [49] and its depletion is a characteristic finding in PD [48,60]. In addition, previous studies have shown altered expression, covalent modifications and decreased activity of glutathione peroxidases in PD brain and models of PD [3,5,27,32,66]. It is also possible that by suppressing other cytoplasmic antioxidant mechanisms such as the peroxiredoxin-thioredoxin system [19,38], α-Synuclein indirectly enhanced glutathione oxidation in response to exogenous peroxide. The influence of α-Synuclein on expression or activity of the relevant enzymes may be an important consideration for understanding our new observations.

We showed previously that α-Synuclein-dependent cell dysfunction precedes cell death following disruption of mitochondrial electron transport [76] and our new data indicate that this early loss of neuronal function correlates with extensive α-Synuclein-dependent thiol oxidation in dopaminergic neurons. In addition, the extensive thiol oxidation we observed in the neuropil adjacent to dopaminergic neurons (Fig. 2B) suggests that the adverse effects of mitochondrial inhibitors in the presence of α-Synuclein extend beyond cellular boundaries, perhaps indicating flux of freely-diffusible hydrogen peroxide outside the cell, or the recruitment of cell non-autonomous mechanisms for ROS production as discussed above. The consequences of enhanced ROS fluxes within neurons are likely wide-ranging and involve oxidative modifications in multiple cellular compartments. Consequently, the cellular targets that account for α-Synuclein-dependent loss of function in dopaminergic neurons following exposure to ETC inhibitors are unclear. However, the detection of oxidatively-stressed neurons with impaired function prior

to neurodegeneration suggests that interventions targeting α-Synuclein-dependent ROS fluxes might provide a means to rescue dysfunctional cells, potentially averting clinical progression after initial presentation. One conceptual approach to this putative therapeutic strategy involves targeting α-Synuclein expression directly. We previously showed that decreasing α-Synuclein in the substantia nigra by ≈ 30% mitigated neurodegeneration in the rat rotenone model [76] and our more recent study found that > 70% α-Synuclein knockdown was tolerated by adult substantia nigra neurons for extended time periods [75]. However, it is still unclear whether gene targeting can be implemented safely and effectively in order to test the efficacy of this approach in patients; furthermore, neurosurgical interventions to infuse vectors into the brain, or serial lumbar punctures to administer antisense oligonucleotides, are likely to be unsuitable for many PD patients. The present study provides a new avenue of investigation. Defining the molecular mechanisms underlying α-Synuclein-dependent peroxide fluxes in dopaminergic neurons *in vivo*, exploiting the chemically- and genetically-tractable zebrafish model, may identify targets for small molecule inhibitors that can prevent progression from oxidatively-stressed dysfunctional neurons to cell death. Studies to define the relevant biochemical events are consequently an important priority.

Declaration of competing interest

There is no conflict of interest.

Acknowledgements

This work was supported by research grants from the National Institutes of Health (ES022644), the U.S. Department of Veterans Affairs (BX000548), and the Pittsburgh Foundation (#M2005-0071). The sponsors had no role in study design, collection, analysis, or interpretation of data, writing the manuscript, or the decision to submit this article for publication. The contents of this article do not represent the views of the United States Government.

Appendix A. Supplementary data

Supplementary data to this article can be found online at https://doi.org/10.1016/j.redox.2020.101695.

Transparency document

Transparency document related to this article can be found online at https://doi.org/10.1016/j.redox.2020.101695

References

[1] M. Baba, S. Nakajo, P.H. Tu, T. Tomita, K. Nakaya, V.M. Lee, J.Q. Trojanowski, T. Iwatsubo, Aggregation of alpha-synuclein in Lewy bodies of sporadic Parkinson's disease and dementia with Lewy bodies, Am. J. Pathol. 152 (1998) 879–884.
[2] W.P. Bartel, V.S. Van Laar, E.A. Burton, Parkinson's disease, in: R.T. Gerlai (Ed.), Behavioral and Neural Genetics of Zebrafish, Elsevier, Academic Press, 2020, pp. 377–412.
[3] F.P. Bellinger, M.T. Bellinger, L.A. Seale, A.S. Takemoto, A.V. Raman, T. Miki, A. B. Manning-Bog, M.J. Berry, L.R. White, G.W. Ross, Glutathione peroxidase 4 is associated with neuromelanin in substantia nigra and dystrophic axons in putamen of Parkinson's brain, Mol. Neurodegener. 6 (2011) 8.
[4] R. Betarbet, T.B. Sherer, G. MacKenzie, M. Garcia-Osuna, A.V. Panov, J. T. Greenamyre, Chronic systemic pesticide exposure reproduces features of Parkinson's disease, Nat. Neurosci. 3 (2000) 1301–1306.
[5] J. Blackinton, R. Kumaran, M.P. van der Brug, R. Ahmad, L. Olson, D. Galter, A. Lees, R. Bandopadhyay, M.R. Cookson, Post-transcriptional regulation of mRNA associated with DJ-1 in sporadic Parkinson disease, Neurosci. Lett. 452 (2009) 8–11.
[6] H. Braak, K. Del Tredici, U. Rub, R.A. de Vos, E.N. Jansen Steur, E. Braak, Staging of brain pathology related to sporadic Parkinson's disease, Neurobiol. Aging 24 (2003) 197–211.
[7] M.D. Brand, Mitochondrial generation of superoxide and hydrogen peroxide as the source of mitochondrial redox signaling, Free Radic. Biol. Med. 100 (2016) 14–31.
[8] J.R. Cannon, V. Tapias, H.M. Na, A.S. Honick, R.E. Drolet, J.T. Greenamyre, A highly reproducible rotenone model of Parkinson's disease, Neurobiol. Dis. 34 (2009) 279–290.
[9] C.L. Cario, T.C. Farrell, C. Milanese, E.A. Burton, Automated measurement of zebrafish larval movement, J. Physiol. 589 (2011) 3703–3708.
[10] N.S. Chandel, D.S. McClintock, C.E. Feliciano, T.M. Wood, J.A. Melendez, A. M. Rodriguez, P.T. Schumacker, Reactive oxygen species generated at mitochondrial complex III stabilize hypoxia-inducible factor-1 alpha during hypoxia: a mechanism of O2 sensing, J. Biol. Chem. 275 (2000) 25130–25138.
[11] M.C. Chartier-Harlin, J. Kachergus, C. Roumier, V. Mouroux, X. Douay, S. Lincoln, C. Levecque, L. Larvor, J. Andrieux, M. Hulihan, et al., Alpha-synuclein locus duplication as a cause of familial Parkinson's disease, Lancet 364 (2004) 1167–1169.
[12] D.H. Choi, A.C. Cristovao, S. Guhathakurta, J. Lee, T.H. Joh, M.F. Beal, Y.S. Kim, NADPH oxidase 1-mediated oxidative stress leads to dopamine neuron death in Parkinson's disease, Antioxidants Redox Signal. 16 (2012) 1033–1045.
[13] N.B. Cole, D. Dieuliis, P. Leo, D.C. Mitchell, R.L. Nussbaum, Mitochondrial translocation of alpha-synuclein is promoted by intracellular acidification, Exp. Cell Res. 314 (2008) 2076–2089.
[14] A.C. Cristovao, S. Guhathakurta, E. Bok, G. Je, S.D. Yoo, D.H. Choi, Y.S. Kim, NADPH oxidase 1 mediates alpha-synucleinopathy in Parkinson's disease, J. Neurosci. 32 (2012) 14465–14477.
[15] M.M. Desouki, M. Kulawiec, S. Bansal, G.M. Das, K.K. Singh, Cross talk between mitochondria and superoxide generating NADPH oxidase in breast and ovarian tumors, Canc. Biol. Ther. 4 (2005) 1367–1373.
[16] L. Devi, V. Raghavendran, B.M. Prabhu, N.G. Avadhani, H. K. Anandatheerthavarada, Mitochondrial import and accumulation of alpha-synuclein impair complex I in human dopaminergic neuronal cultures and Parkinson disease brain, J. Biol. Chem. 283 (2008) 9089–9100.
[17] R. Di Maio, P.J. Barrett, E.K. Hoffman, C.W. Barrett, A. Zharikov, A. Borah, X. Hu, J. McCoy, C.T. Chu, E.A. Burton, et al., alpha-Synuclein binds to TOM20 and inhibits mitochondrial protein import in Parkinson's disease, Sci. Transl. Med. 8 (2016) 342ra378.
[18] A.A. Dukes, Q. Bai, V.S. Van Laar, Y. Zhou, V. Ilin, C.N. David, Z.S. Agim, J. L. Bonkowsky, J.R. Cannon, S.C. Watkins, et al., Live imaging of mitochondrial dynamics in CNS dopaminergic neurons in vivo demonstrates early reversal of mitochondrial transport following MPP(+) exposure, Neurobiol. Dis. 95 (2016) 238–249.
[19] J. Fang, T. Nakamura, D.H. Cho, Z. Gu, S.A. Lipton, S-nitrosylation of peroxiredoxin 2 promotes oxidative stress-induced neuronal cell death in Parkinson's disease, Proc. Natl. Acad. Sci. U. S. A. 104 (2007) 18742–18747.
[20] T.C. Farrell, C.L. Cario, C. Milanese, A. Vogt, J.H. Jeong, E.A. Burton, Evaluation of spontaneous propulsive movement as a screening tool to detect rescue of Parkinsonism phenotypes in zebrafish models, Neurobiol. Dis. 44 (2011) 9–18.
[21] E. Fujimoto, T.J. Stevenson, C.B. Chien, J.L. Bonkowsky, Identification of a dopaminergic enhancer indicates complexity in vertebrate dopamine neuron phenotype specification, Dev. Biol. 352 (2011) 393–404.
[22] M. Gutscher, A.L. Pauleau, L. Marty, T. Brach, G.H. Wabnitz, Y. Samstag, A. J. Meyer, T.P. Dick, Real-time imaging of the intracellular glutathione redox potential, Nat. Methods 5 (2008) 553–559.
[23] M. Gutscher, M.C. Sobotta, G.H. Wabnitz, S. Ballikaya, A.J. Meyer, Y. Samstag, T. P. Dick, Proximity-based protein thiol oxidation by H2O2-scavenging peroxidases, J. Biol. Chem. 284 (2009) 31532–31540.
[24] R.H. Haas, F. Nasirian, K. Nakano, D. Ward, M. Pay, R. Hill, C.W. Shults, Low platelet mitochondrial complex I and complex II/III activity in early untreated Parkinson's disease, Ann. Neurol. 37 (1995) 714–722.
[25] T.G. Hastings, The role of dopamine oxidation in mitochondrial dysfunction: implications for Parkinson's disease, J. Bioenerg. Biomembr. 41 (2009) 469–472.
[26] T.G. Hastings, D.A. Lewis, M.J. Zigmond, Role of oxidation in the neurotoxic effects of intrastriatal dopamine injections, Proc. Natl. Acad. Sci. U. S. A. 93 (1996) 1956–1961.
[27] D.N. Hauser, A.A. Dukes, A.D. Mortimer, T.G. Hastings, Dopamine quinone modifies and decreases the abundance of the mitochondrial selenoprotein glutathione peroxidase 4, Free Radic. Biol. Med. 65 (2013) 419–427.
[28] M.P. Horowitz, C. Milanese, R. Di Maio, X. Hu, L.M. Montero, L.H. Sanders, V. Tapias, S. Sepe, W.A. van Cappellen, E.A. Burton, et al., Single-cell redox imaging demonstrates a distinctive response of dopaminergic neurons to oxidative insults, Antioxid. Redox Signal. 15 (2011) 855–871.
[29] L. Hou, X. Bao, C. Zang, H. Yang, F. Sun, Y. Che, X. Wu, S. Li, D. Zhang, Q. Wang, Integrin CD11b mediates alpha-synuclein-induced activation of NADPH oxidase through a Rho-dependent pathway, Redox Biol 14 (2018) 600–608.
[30] J.A. Javitch, R.J. D'Amato, S.M. Strittmatter, S.H. Snyder, Parkinsonism-inducing neurotoxin, N-methyl-4-phenyl-1,2,3,6 -tetrahydropyridine: uptake of the metabolite N-methyl-4-phenylpyridine by dopamine neurons explains selective toxicity, Proc. Natl. Acad. Sci. U. S. A. 82 (1985) 2173–2177.
[31] T. Jiang, J. Hoekstra, X. Heng, W. Kang, J. Ding, J. Liu, S. Chen, J. Zhang, P2X7 receptor is critical in alpha-synuclein–mediated microglial NADPH oxidase activation, Neurobiol. Aging 36 (2015) 2304–2318.
[32] S.J. Kish, C. Morito, O. Hornykiewicz, Glutathione peroxidase activity in Parkinson's disease brain, Neurosci. Lett. 58 (1985) 343–346.
[33] J.H. Kordower, R.E. Burke, Disease modification for Parkinson's disease: axonal regeneration and trophic factors, Mov. Disord. 33 (2018) 678–683.

[34] R. Kruger, W. Kuhn, T. Muller, D. Woitalla, M. Graeber, S. Kosel, H. Przuntek, J. T. Epplen, L. Schols, O. Riess, Ala30Pro mutation in the gene encoding alpha-synuclein in Parkinson's disease, Nat. Genet. 18 (1998) 106–108.
[35] A.M. Lambert, J.L. Bonkowsky, M.A. Masino, The conserved dopaminergic diencephalospinal tract mediates vertebrate locomotor development in zebrafish larvae, J. Neurosci. 32 (2012) 13488–13500.
[36] J.W. Langston, P. Ballard, J.W. Tetrud, I. Irwin, Chronic Parkinsonism in humans due to a product of meperidine-analog synthesis, Science 219 (1983) 979–980.
[37] S.B. Lee, I.H. Bae, Y.S. Bae, H.D. Um, Link between mitochondria and NADPH oxidase 1 isozyme for the sustained production of reactive oxygen species and cell death, J. Biol. Chem. 281 (2006) 36228–36235.
[38] Y.M. Lee, S.H. Park, D.I. Shin, J.Y. Hwang, B. Park, Y.J. Park, T.H. Lee, H.Z. Chae, B.K. Jin, T.H. Oh, et al., Oxidative modification of peroxiredoxin is associated with drug-induced apoptotic signaling in experimental models of Parkinson disease, J. Biol. Chem. 283 (2008) 9986–9998.
[39] W.G. Li, F.J. Miller Jr., H.J. Zhang, D.R. Spitz, L.W. Oberley, N.L. Weintraub, H(2)O(2)-induced O(2) production by a non-phagocytic NAD(P)H oxidase causes oxidant injury, J. Biol. Chem. 276 (2001) 29251–29256.
[40] W.W. Li, R. Yang, J.C. Guo, H.M. Ren, X.L. Zha, J.S. Cheng, D.F. Cai, Localization of alpha-synuclein to mitochondria within midbrain of mice, Neuroreport 18 (2007) 1543–1546.
[41] K.C. Luk, V.M. Kehm, B. Zhang, P. O'Brien, J.Q. Trojanowski, V.M. Lee, Intracerebral inoculation of pathological α-synuclein initiates a rapidly progressive neurodegenerative α-synucleinopathy in mice, J. Exp. Med. 209 (2012) 975–986.
[42] E.S. Luth, I.G. Stavrovskaya, T. Bartels, B.S. Kristal, D.J. Selkoe, Soluble, prefibrillar alpha-synuclein oligomers promote complex I-dependent, Ca2+-induced mitochondrial dysfunction, J. Biol. Chem. 289 (2014) 21490–21507.
[43] A.J. Meyer, T.P. Dick, Fluorescent protein-based redox probes, Antioxidants Redox Signal. 13 (2010) 621–650.
[44] C. Milanese, J.J. Sager, Q. Bai, T.C. Farrell, J.R. Cannon, J.T. Greenamyre, E. A. Burton, Hypokinesia and reduced dopamine levels in zebrafish lacking beta- and gamma1-synucleins, J. Biol. Chem. 287 (2012) 2971–2983.
[45] S. Mittal, K. Bjornevik, D.S. Im, A. Flierl, X. Dong, J.J. Locascio, K.M. Abo, E. Long, M. Jin, B. Xu, et al., beta2-Adrenoreceptor is a regulator of the alpha-synuclein gene driving risk of Parkinson's disease, Science 357 (2017) 891–898.
[46] D. Narendra, A. Tanaka, D.F. Suen, R.J. Youle, Parkin is recruited selectively to impaired mitochondria and promotes their autophagy, J. Cell Biol. 183 (2008) 795–803.
[47] D.P. Narendra, S.M. Jin, A. Tanaka, D.F. Suen, C.A. Gautier, J. Shen, M.R. Cookson, R.J. Youle, PINK1 is selectively stabilized on impaired mitochondria to activate Parkin, PLoS Biol. 8 (2010), e1000298.
[48] R.K. Pearce, A. Owen, S. Daniel, P. Jenner, C.D. Marsden, Alterations in the distribution of glutathione in the substantia nigra in Parkinson's disease, J. Neural. Transm. 104 (1997) 661–677.
[49] T.L. Perry, D.V. Godin, S. Hansen, Parkinson's disease: a disorder due to nigral glutathione deficiency? Neurosci. Lett. 33 (1982) 305–310.
[50] M.H. Polymeropoulos, C. Lavedan, E. Leroy, S.E. Ide, A. Dehejia, A. Dutra, B. Pike, H. Root, J. Rubenstein, R. Boyer, et al., Mutation in the alpha-synuclein gene identified in families with Parkinson's disease, Science 276 (1997) 2045–2047.
[51] E. Provost, J. Rhee, S.D. Leach, Viral 2A peptides allow expression of multiple proteins from a single ORF in transgenic zebrafish embryos, Genesis 45 (2007) 625–629.
[52] C.L. Quinlan, R.L. Goncalves, M. Hey-Mogensen, N. Yadava, V.I. Bunik, M. D. Brand, The 2-oxoacid dehydrogenase complexes in mitochondria can produce superoxide/hydrogen peroxide at much higher rates than complex I, J. Biol. Chem. 289 (2014) 8312–8325.
[53] R.R. Ramsay, M.J. Krueger, S.K. Youngster, M.R. Gluck, J.E. Casida, T.P. Singer, Interaction of 1-methyl-4-phenylpyridinium ion (MPP+) and its analogs with the rotenone/piericidin binding site of NADH dehydrogenase, J. Neurochem. 56 (1991) 1184–1190.
[54] E. Rink, M.F. Wullimann, The teleostean (zebrafish) dopaminergic system ascending to the subpallium (striatum) is located in the basal diencephalon (posterior tuberculum), Brain Res. 889 (2001) 316–330.
[55] W. Satake, Y. Nakabayashi, I. Mizuta, Y. Hirota, C. Ito, M. Kubo, T. Kawaguchi, T. Tsunoda, M. Watanabe, A. Takeda, et al., Genome-wide association study identifies common variants at four loci as genetic risk factors for Parkinson's disease, Nat. Genet. 41 (2009) 1303–1307.
[56] A.H. Schapira, J.M. Cooper, D. Dexter, P. Jenner, J.B. Clark, C.D. Marsden, Mitochondrial complex I deficiency in Parkinson's disease, Lancet 1 (1989) 1269.
[57] S. Shavali, H.M. Brown-Borg, M. Ebadi, J. Porter, Mitochondrial localization of alpha-synuclein protein in alpha-synuclein overexpressing cells, Neurosci. Lett. 439 (2008) 125–128.
[58] T.B. Sherer, R. Betarbet, C.M. Testa, B.B. Seo, J.R. Richardson, J.H. Kim, G. W. Miller, T. Yagi, A. Matsuno-Yagi, J.T. Greenamyre, Mechanism of toxicity in rotenone models of Parkinson's disease, J. Neurosci. 23 (2003) 10756–10764.
[59] T.B. Sherer, J.H. Kim, R. Betarbet, J.T. Greenamyre, Subcutaneous rotenone exposure causes highly selective dopaminergic degeneration and alpha-synuclein aggregation, Exp. Neurol. 179 (2003) 9–16.
[60] J. Sian, D.T. Dexter, A.J. Lees, S. Daniel, Y. Agid, F. Javoy-Agid, P. Jenner, C. D. Marsden, Alterations in glutathione levels in Parkinson's disease and other neurodegenerative disorders affecting basal ganglia, Ann. Neurol. 36 (1994) 348–355.
[61] J. Simon-Sanchez, C. Schulte, J.M. Bras, M. Sharma, J.R. Gibbs, D. Berg, C. Paisan-Ruiz, P. Lichtner, S.W. Scholz, D.G. Hernandez, et al., Genome-wide association study reveals genetic risk underlying Parkinson's disease, Nat. Genet. 41 (2009) 1308–1312.
[62] A.B. Singleton, M. Farrer, J. Johnson, A. Singleton, S. Hague, J. Kachergus, M. Hulihan, T. Peuralinna, A. Dutra, R. Nussbaum, et al., alpha-Synuclein locus triplication causes Parkinson's disease, Science 302 (2003) 841.
[63] M.G. Spillantini, M.L. Schmidt, V.M. Lee, J.Q. Trojanowski, R. Jakes, M. Goedert, Alpha-synuclein in Lewy bodies, Nature 388 (1997) 839–840.
[64] Z. Sun, A.D. Gitler, Discovery and characterization of three novel synuclein genes in zebrafish, Dev. Dynam. 237 (2008) 2490–2495.
[65] C.M. Tanner, F. Kamel, G.W. Ross, J.A. Hoppin, S.M. Goldman, M. Korell, C. Marras, G.S. Bhudhikanok, M. Kasten, A.R. Chade, et al., Rotenone, paraquat, and Parkinson's disease, Environ. Health Perspect. 119 (2011) 866–872.
[66] V.S. Van Laar, A.J. Mishizen, M. Cascio, T.G. Hastings, Proteomic identification of dopamine-conjugated proteins from isolated rat brain mitochondria and SH-SY5Y cells, Neurobiol. Dis. 34 (2009) 487–500.
[67] S. Wang, C.H. Chu, M. Guo, L. Jiang, H. Nie, W. Zhang, B. Wilson, L. Yang, T. Stewart, J.S. Hong, et al., Identification of a specific alpha-synuclein peptide (alpha-Syn 29-40) capable of eliciting microglial superoxide production to damage dopaminergic neurons, J. Neuroinflammation 13 (2016) 158.
[68] C.J. Weaver, Y.F. Leung, D.M. Suter, Expression dynamics of NADPH oxidases during early zebrafish development, J. Comp. Neurol. 524 (2016) 2130–2141.
[69] R.M. White, A. Sessa, C. Burke, T. Bowman, J. LeBlanc, C. Ceol, C. Bourque, M. Dovey, W. Goessling, C.E. Burns, et al., Transparent adult zebrafish as a tool for in vivo transplantation analysis, Cell Stem Cell 2 (2008) 183–189.
[70] C.S. Wilcox, Effects of tempol and redox-cycling nitroxides in models of oxidative stress, Pharmacol. Ther. 126 (2010) 119–145.
[71] M.T. Woodlee, J.R. Kane, J. Chang, L.K. Cormack, T. Schallert, Enhanced function in the good forelimb of hemi-Parkinson rats: compensatory adaptation for contralateral postural instability? Exp. Neurol. 211 (2008) 511–517.
[72] D.C. Wu, P. Teismann, K. Tieu, M. Vila, V. Jackson-Lewis, H. Ischiropoulos, S. Przedborski, NADPH oxidase mediates oxidative stress in the 1-methyl-4-phenyl-1,2,3,6-tetrahydropyridine model of Parkinson's disease, Proc. Natl. Acad. Sci. U. S. A. 100 (2003) 6145–6150.
[73] W. Xie, B. Jiao, Q. Bai, V.A. Ilin, M. Sun, C.E. Burton, D. Kolodieznyi, M. J. Calderon, D.B. Stolz, P.L. Opresko, et al., Chemoptogenetic ablation of neuronal mitochondria in vivo with spatiotemporal precision and controllable severity, eLife 9 (2020), e51845.
[74] W.M. Zawada, R.E. Mrak, J. Biedermann, Q.D. Palmer, S.M. Gentleman, O. Aboud, W.S. Griffin, Loss of angiotensin II receptor expression in dopamine neurons in Parkinson's disease correlates with pathological progression and is accompanied by increases in Nox4- and 8-OH guanosine-related nucleic acid oxidation and caspase-3 activation, Acta Neuropathologica Commun. 3 (2015) 9.
[75] A. Zharikov, Q. Bai, B.R. De Miranda, A. Van Laar, J.T. Greenamyre, E.A. Burton, Long-term RNAi knockdown of alpha-synuclein in the adult rat substantia nigra without neurodegeneration, Neurobiol. Dis. 125 (2019) 146–153.
[76] A.D. Zharikov, J.R. Cannon, V. Tapias, Q. Bai, M.P. Horowitz, V. Shah, A. El Ayadi, T.G. Hastings, J.T. Greenamyre, E.A. Burton, shRNA targeting alpha-synuclein prevents neurodegeneration in a Parkinson's disease model, J. Clin. Invest. 125 (2015) 2721–2735.
[77] Y. Zhou, R.T. Cattley, C.L. Cario, Q. Bai, E.A. Burton, Quantification of larval zebrafish motor function in multiwell plates using open-source MATLAB applications, Nat. Protoc. 9 (2014) 1533–1548.